A KALMAN FILTER BASED ALGORITHM FOR ENHANCING ACCURACY OF KILN ROLLER BEARING TEMPERATURE MEASUREMENTS IN CEMENT PRODUCTION AT HIMA CEMENT PLANT

BY

AHEBWA SAMUEL

(B. Eng. Ind. Eng. & Mgt., Kyu)

22/U/GMEM/017/PE

A DISSERTATION SUBMITTED TO THE DIRECTORATE OF RESEARCH AND GRADUATE TRAINING IN PARTIAL FULFILLMENT OF THE REQUIREMENTS FOR THE AWARD OF THE DEGREE OF MASTER OF SCIENCE IN ADVANCED MANUFACTURING SYSTEMS ENGINEERING OF KYAMBOGO UNIVERSITY

OCTOBER, 2025

DECLARATION

I, Ahebwa Samuel, do hereby affirm that I am the sole author of every aspect of this dissertation contained herein describing my involvement as a student of MSc. Advanced Manufacturing Systems Engineering and has not been submitted to any other University before or any other institution with regard to any award. All information contained herein is thus certain and truthful of my effort.

Signature …… Date ……

APPROVAL

This is to verify that the work included in this dissertation was entirely written by Mr. Ahebwa Samuel, a Master's student and was authentically carried out under my supervision.

Date:…… Signature:……

Dr. Kangwagye Samuel

Date:……..… Signature:……

Dr. Maureen Nalubowa Ssempija

DEDICATION

This Master's dissertation is dedicated to my family who have served as my pillar of positive reinforcement throughout this ordeal and shaped me towards the person that I am today.

I am greatly indebted to my supervisors and mentors, whose inspiration and priceless insight have driven my quest for knowledge.

To my acquaintances and coworkers, thank you for your cooperation and motivation that made this venture exceedingly rewarding.

And to everyone who believed in me, thank you for being a part of my story. Your impact and unshakable faith in my potential are demonstrated by this effort.

ACKNOWLEDGMENT

Firstly, I want to convey sincere appreciation to my supervisors, Dr. Kangwagye Samuel and Dr. Maureen Nalubowa Ssempija, for their expert advice, insightful feedback and continuous support throughout this dissertation.

I am thankful to the entire faculty of Kyambogo University's Department of Mechanical and Production Engineering for their expertise and resources in making this research feasible.

I want to express my gratitude to Hima Cement Limited's management and the employees for letting me carry out this research at the facility.

Special thanks to my peers, whose collaboration and constructive discussions provided fresh perspectives and fueled my determination to see this research through. To my friends, who have cheered me on and offered their support during challenging times, thank you for always being there.

Finally, I would like to express my most profound appreciation to my family for their constant prayers, love, encouragement, and patience all through this entire ordeal. Your faith in me has been my most powerful source of strength. This work would not have been possible without each of you.

TABLE OF CONTENTS

LIST OF FIGURES

LIST OF TABLES

LIST OF ACRONYMS

KF	Kalman Filter
RK3	Rotary Kiln 3
IR	Infrared
NWP	Numerical Weather Prediction
ECMWF	European Centre for Medium-Range Weather Forecasts
EKF	Extended Kalman Filter
UKF	Unscented Kalman Filter
EnKF	Ensemble Kalman Filter
SPSS	Statistical Package for the Social Sciences

ABSTRACT

A rotary kiln is an integral component of a cement production plant mounted on tire/roller assemblies and supported by partial journal bearings. Temperature monitoring of the bearings is necessary to prevent unexpected damage. The rotary kiln (RK3) at Hima Cement Factory operates with a discrepancy in roller bearing temperature measurements typically between Hand Pyrometer Readings and Control room readings, ranging from 0.1◦C to 44◦C. This deviation in measurements can be attributed to abrupt sensor failures caused by power issues, loose contacts, or data system flaws as well as flying particulate matter inside the kiln system obscures the sensor. While there is a potential risk of tripping the kiln main drive on interlock due to undetected temperatures that are out of operational range, kiln roller bearings are also likely to deteriorate when operated at high temperatures for a long time. The intention of the research was to create a Kalman Filter-based algorithm that provides more accurate estimates of kiln roller bearing temperatures.The proposed method's accuracy was validated by comparing actual measurements obtained under controlled test conditions with ground truth obtained by HPR. The experiment then tested whether the Extended Kalman Filter can reduce noise, adapt to dynamic changes, and provide estimates that are close to the ground truth. The study showed a 94% improvement in temperature measurement accuracy under noisy conditions, reducing the initial RMSE from 8.656°C towards 0.523°C and MAE from 8.060°C towards 0.445°C after Kalman correction. This increased the reliability of temperature monitoring in dynamic environments. Implementing a real-time monitoring system is critical to ensuring that the Kalman filter functions with current and correct data while configuring a comprehensive alarm system to ensure safety and efficiency in the cement rotary kiln operations.

CHAPTER ONE:INTRODUCTION

1.1 Background

A rotary kiln is a low-speed, heavy-duty, large-scale calcining equipment. It is commonly utilized in the chemical, metallurgy, and building materials industries. (L. Liu et al., 2024) Producing cement involves pulverizing a mixture of limestone, shale, clay, sand, and lesser amounts of other components in precise ratios to a fine powder and burning raw cement produced within a large rotary kiln (Matias et al., 2013) The cement kiln is the most critical component of the cement manufacturing process, producing cement clinker (Saidur et al., 2011) This kiln shell is attached to the tire - roller assembly at several locations, which is sustained by partial journal bearings (Effect et al., 2019) Bearings are exposed to tough field conditions year-round in order to keep productive progress smooth and minimize unplanned downtime, it is vital to monitor their status in real time. Premature bearing failure occurs under harsh working conditions such as heavy loads, very fast speed, and very high or low operating temperatures (Shelke & Galhe, 2016) Being basically a pyro process, the importance of temperature measurements for kiln control is obvious (Wahidmurni, 2017) Because measuring temperature by touch is difficult, a pyrometer is used instead. However, numerous readings include inaccuracies because flying particles within the cement kiln hide the sensor (Matias et al., 2013) The Kalman filter was first employed in Apollo and then has been also utilized in guided navigation, nuclear plant instrumentation, demography modeling, manufacturing, as well as parameter identification, robot control, and navigational autonomy. (Urrea & Agramonte, 2021). This study is limited in cement production and thus proposes an EKF filter based algorithm to enhance the accuracy of kiln roller bearing temperature measurements.

1.2 Description of the Temperature Monitoring Problem on the Kiln

Consider a case of Hima Cement Plant, Kasese. The plant has three production lines; 1, 2 and 3, each with a Rotary Kiln. Of the 3 lines, only 2 and 3 are operational while line 1 was decommissioned. The focus is on Rotary Kiln 3 (RK3) in Figure 1.1. During operations, accurate temperature monitoring for RK3 roller bearings at different kiln tires is crucial for preventing equipment failure and ensuring operational safety. Operational temperatures at 50◦C raise a warning alarm while beyond 75◦C, the system is programmed to initiate a kiln trip.

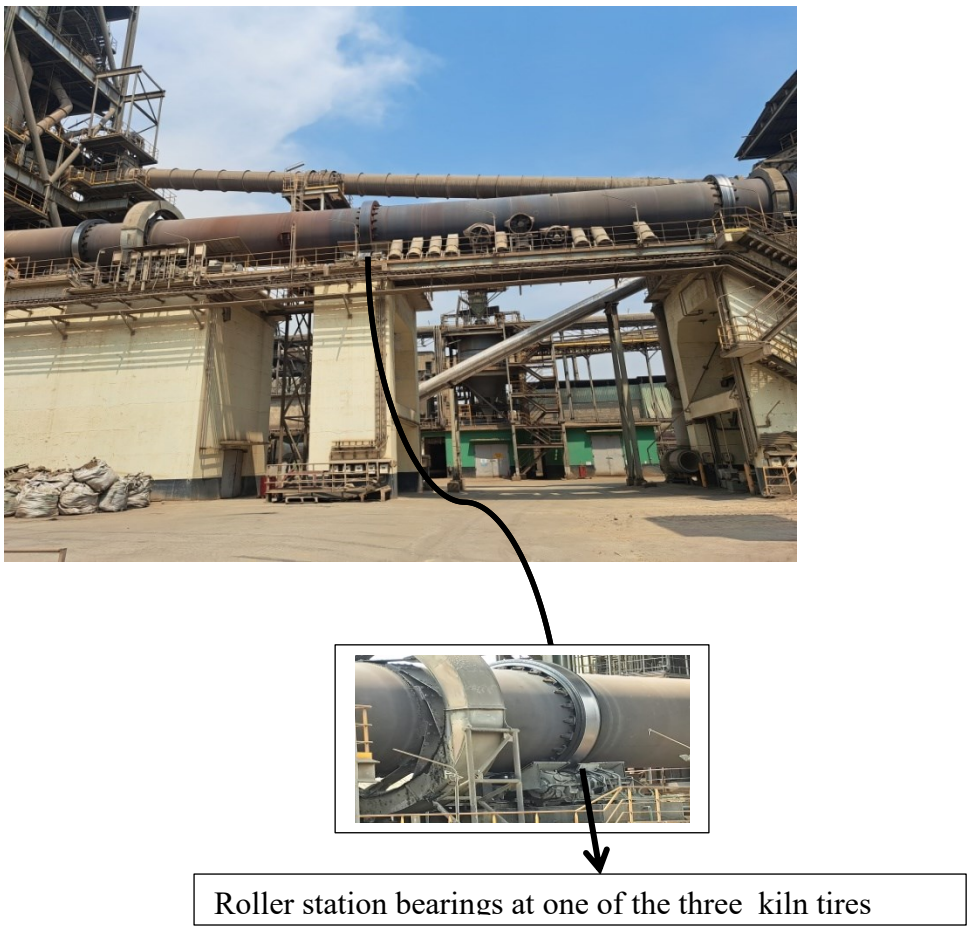

Figure 1.1: A photo of RK3 at Hima Cement Plant

However, a persistent challenge is a discrepancy in kiln roller temperatures between the control room noisy sensor readings and hand pyrometer measurements, typically ranging

from 0.1◦C to 44◦C. While there is a potential risk of tripping the kiln main drive on interlock due to undetected temperatures out of operational range of 0◦C to 75◦C, kiln roller bearings are also likely to deteriorate when operated at elevated temperatures for a long time. *Figure 1.2 (a)* is a rotary kiln (CCR) supported by an assembly of roller stations at three different tires as shown.

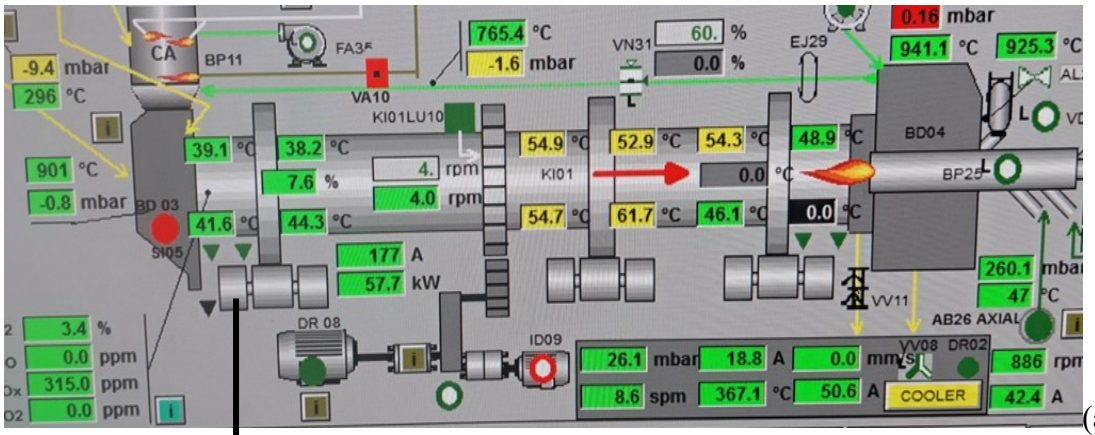

(a)

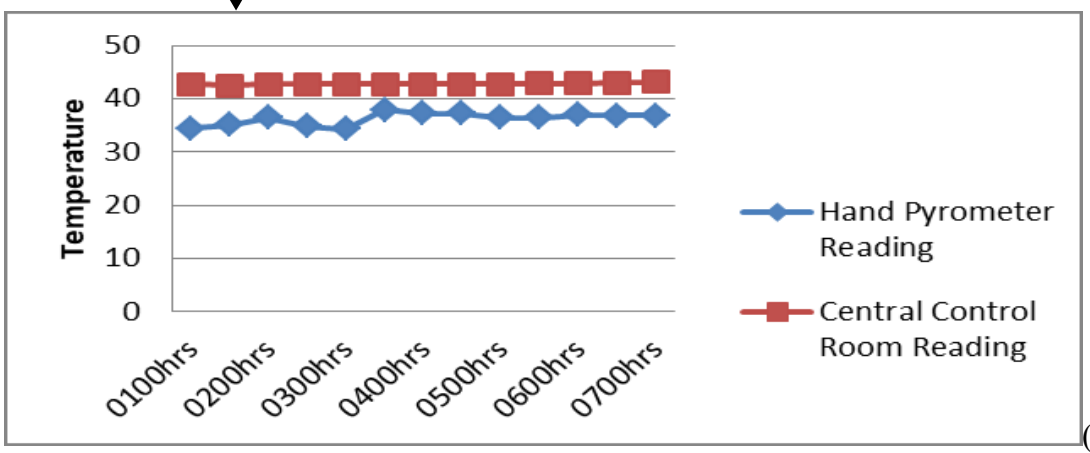

(b)

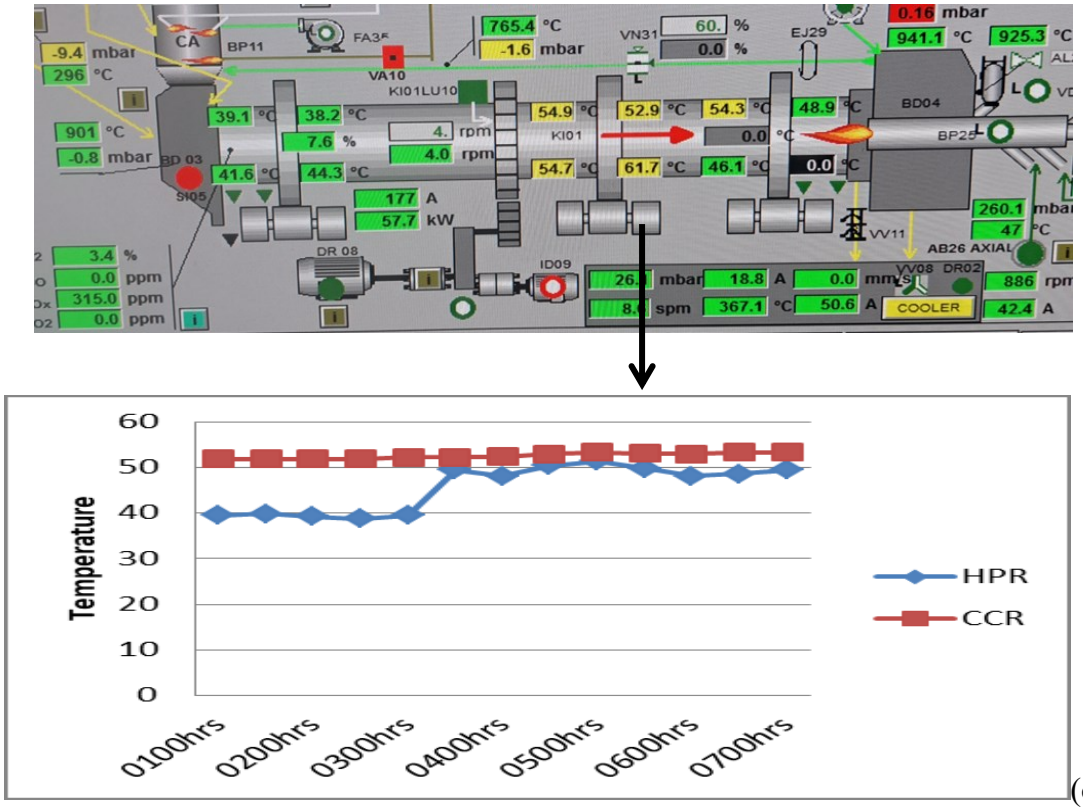

(c)

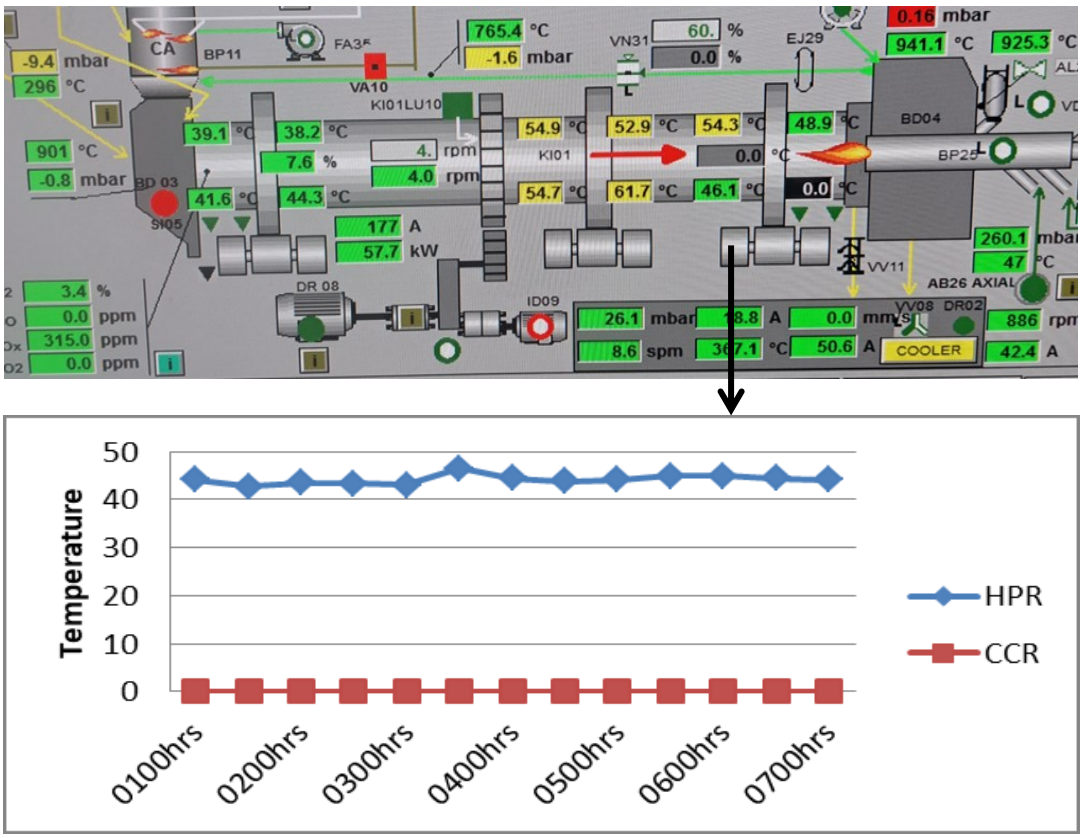

(d)

Figure 1.2: Temperature readings taken from different bearings at different kiln tires (support stations)

Temperature readings were taken for each of the four bearings at the different kiln roller stations by using a fluke hand pyrometer in time intervals of 30 minutes. At the same time interval, control room display readings (CCR) were taken as well for comparison purposes with Hand Pyrometer Readings (HPR) as ground truth. Significant error margins in bearing temperature measurements were realized. *Figure 1.2 (b)* and *(c)* which are representations of particular roller bearings indicated higher central control room readings than the ground truth for the entire period of production with an error magnitude of 6.5◦C and 7◦C respectively. Conversely, *(d)* indicated a higher ground truth compared to the central control room readings with a 44◦C error magnitude. Figure 1.3 shows the magnitude in error of the three bearings under consideration as discussed above.

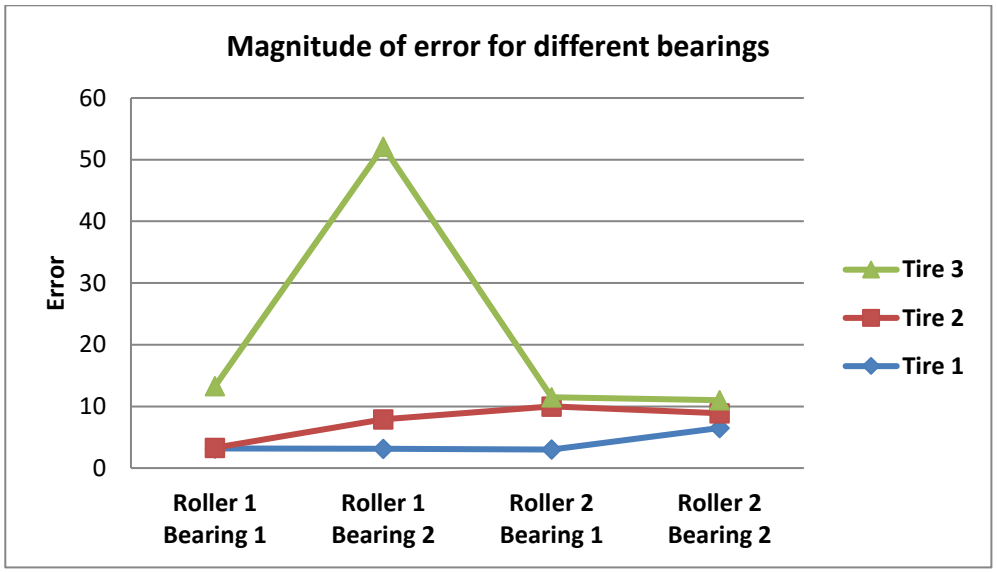

Figure 1.3:Magnitude of error for different bearings at different roller stations

The inconsistencies in temperature measurements could stem from various factors including sensor measurement errors, data transmission inaccuracies, sensor defects etc. Such discrepancies may hinder preventative maintenance strategies.

1.3 Problem Statement

Temperature discrepancies between ground truth and control room readings, ranging from 0.1°C to 44°C, are problematic causing kiln drive trips on interlock above operating thresholds of 75◦C in RK3 operations at Hima Cement Plant, Kasese as shown in Figure 1.3. A temperature sensor malfunction may result in poor thermal control. (Dey et al., 2016). Power concerns, loose contacts, or data system faults can all cause sudden failures; however, emerging sensor malfunctions, like drift, are more challenging to detect (Mosallaei et al., n.d.) Furthermore, flying particulate inside the fired up kiln could block the pyrometer sensor, causing temperature sensing difficulties (Matias et al., 2013). This could result into unreliable temperature readings causing bearings to overheat and fail prematurely. Sensor faults result in significant economic losses during the industrial manufacturing process (Han et al., 2019).

1.4 Objectives

1.4.1 Main Objective

To develop a Kalman Filter Based Algorithm for Enhancing Accuracy of Kiln Roller Bearing Temperature Measurements in Cement Production

1.4.2 Specific objectives

i. To derive a mathematical model describing the dynamics of temperature changes over time in the rotary kiln.

ii. To incorporate the system model and measurement data in an existing Kalman filter framework for accurate temperature estimation

iii. To validate the method's accuracy offline using raw measurements obtained from the Kiln.

1.5 Research Questions

i. How can the dynamic model of the cement rotary kiln be modeled?

ii. How can a Kalman filter framework be used to integrate the model and measurement data for precise temperature estimation?

iii. How accurate is the proposed method when compared to raw kiln temperature measurements?

1.6 Justification

To ensure the safety and reliability of rotary kilns, accurate temperature monitoring of the kiln roller bearings is required, as bearing overheating is a major contributor to premature failure, unexpected downtime, and costly repairs. Excessive reliance on irregular data can lead to catastrophic breakdowns if maintenance is delayed or unnecessary and costly interventions if false alarms are triggered. This study focuses on the intrinsic discrepancy and noisiness of temperature sensor readings, which presents a considerable maintenance challenge. To solve this, the current study creates and evaluates an advanced algorithmic approach designed to integrate data from kiln roller bearings at the three different tire stations.

1.7 Scope

This project research is carried out at Hima Cement Limited, a cement-producing company located in Kasese district, Western Region of Uganda. The plant is located about 23km and 350km by road from Kasese and Kampala respectively. This research aimed at developing a Kalman Filter based algorithm for temperature measurement enhancement. Temperature data is gathered from kiln roller station bearings and the developed algorithm is tested offline with this data to confirm its validity in estimating the temperature measurements.

1.7 Conceptual Framework

Measurement process explored how the temperature readings were observed, recorded, and analyzed. This included understanding the sources of measurement errors and strategies for error minimization. The principles of signal processing relevant to temperature measurements and details the Kalman Filter's role in predicting and correcting measurement errors to enhance accuracy were also deployed in the study. The conceptual framework model depicted in **Figure 1.4** depicts the various research variables and their interactions.

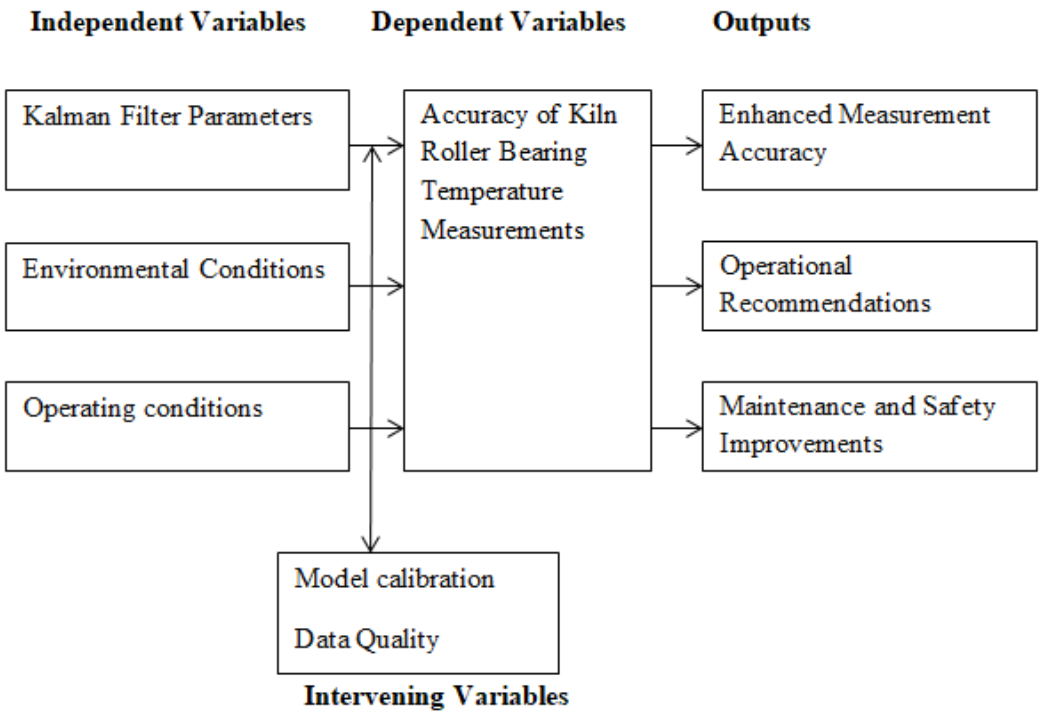

Figure 1.4: Conceptual framework of the study

CHAPTER TWO: LITERATURE REVIEW

2.1 Modeling of Rotary Kiln Temperature Dynamics

2.1.1 Cement Production Process Overview

Cement manufacture begins with the extraction of raw materials, followed by pre-crushing in a quarry adjacent to the cement factory. When the ratio of raw materials is precisely established, a mixture is made, if necessary, by adding correction elements such as sand, iron ore, and clay (Cipurkovic et al., 2014) The function of the cement kiln is to convert the cement raw material that has been ground into fine powder into a cement clinker under high-temperature conditions (Wei et al., 2020). Rotary kiln is a vital component in cement manufacturing. It is a type of heavy load, large torque, multi-support, and unstable redundancy system. The operating status will affect the efficiency and safety of the whole production line directly (Hu & Guo, 2016). Since the main reactions related to clinkerisation happen in the rotary kiln, the cement kiln's operating efficiency manages the cement standards and entire plant operation. (Mujumdar & Ranade, 2006). **Figure 2.1** depicts a visual representation of the cement production process.

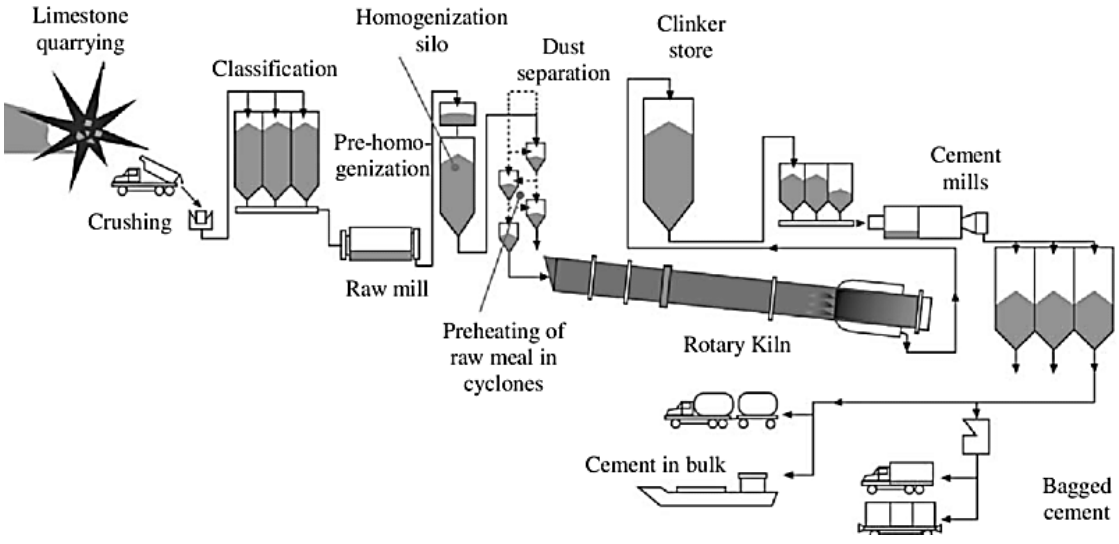

Figure 2.1: Schematic diagram for a cement manufacturing process (Rahman et al., 2013)

To support the rotary kiln, each roller station requires two supporting rollers with the appropriate supporting roller bearings, as well as the related base plates. (*Simple Bearing Replacement , Designed for Easy Mounting*, n.d.). **Figure 2.2** is a typical representation of a three roller station rotary kiln mounted on three piers to transmit excess load into the ground. Also as part of the assembly is the girth gear to transmit motion from the main drive to the kiln

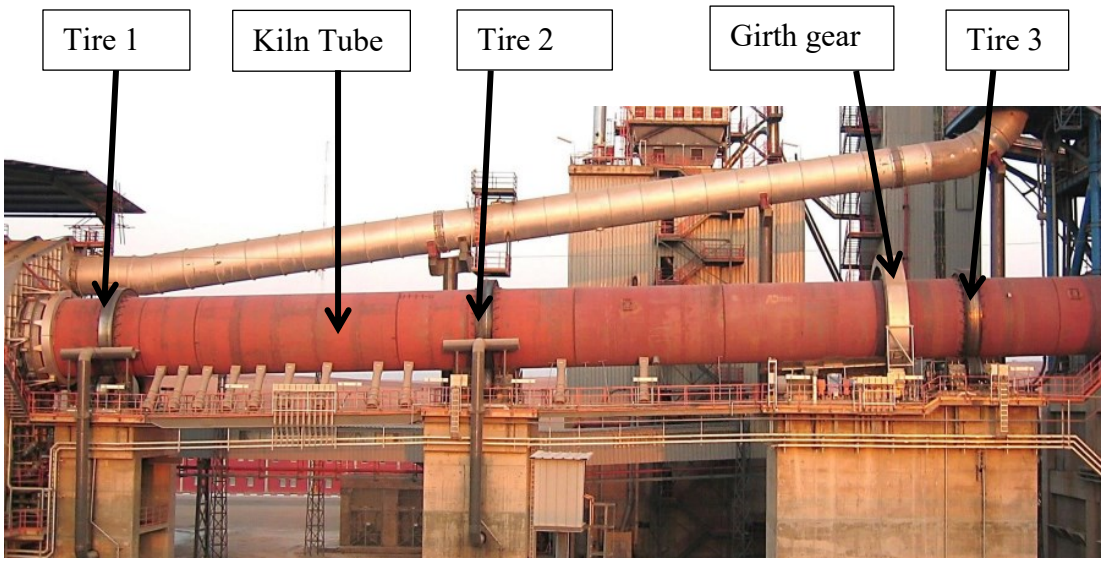

Figure 2.2: Kiln mounted on the three piers (Tools & Industry, n.d.)

2.1.2 Heat Transfer Mechanisms in Rotary Kilns

Heat and mass conveyance throughout a revolving kiln comes with diverse uses in industrial processes such as the manufacture of organic or mineral compounds (Mungyeko & Huchet, 2023). A rotational kiln with a diameter of several meters and a length of 100 meters is used to create lime, cement, titanium dioxide, and alumina at temperatures spanning from 800°C to 1500°C (Ouyang et al., n.d.). Heat exchanges in a fired revolving kiln usually take place three classic ways of heat transfer: conduction, convection, and radiation, as well as between the three fundamental components, which

are the solid section of the bed, walls, and the gas that exists (Mungyeko Bisulandu & Huchet, 2023).

Assuming that the temperature distribution T is known, Hasfjord, 2014 evaluated heat transmission using rate equations. The rate equation for conduction, dubbed **Fourier's law**, can be expressed for a plane this way:

$$q''_{conduction} = = - k \Delta T \quad (2.1)$$

In this equation, q'' equates to the heat flux [W/m^2] and k refers to the thermal conductivity [W/m^2].

Newton's law of cooling, which is the regulating rate equation for convection, ought to be expressed as;

$$q''_{convection} = h_c (T_s - T_\infty) \quad (2.2)$$

Given T_s and T_l being the surface temperature and the fluid (K) respectively, while h is the coefficient of convection heat transfer.

Inbound radiation aimed at a surface can be taken in or rebounded; when taken in, the surface's thermal energy increases, and when rebounded, the radiation returns to the environment. **The Stephan-Boltzmann law** governs the rate equation and is defined here for a grey surface.

$$q''_{radiation} = \varepsilon \sigma (T_s^4 - T_{sur}^4) \quad (2.3)$$

Where $0 \leq \varepsilon \leq 1$ is the surface emissivity, σ is the Stephan-Boltzmann constant, T_s and T_{sur} is the temperature at the radiating surface and the surrounding surface, respectively.

Heat transfer between the underneath of the solid bed and the inside wall that it covers plays an essential role in the overall transfer process as shown in **Figure 2.3**. While this result is conceptually expressed right here as conductive heat transfer because of the proximity placement of the bed and wall, all three predominant forms of heat transmission within this scenario are actually conduction through the gas film between the wall and the bed, advective heat transfer near the bed margins, and direct solid-wall contact conduction. (Hanein, 2017) Heat transmission via convection is considered to follow Newton's Law of Cooling stipulates that an object's rate of heat loss correlates to the temperature gradient between it and its environment (Jain, 2024).

The thermal system model is built on thermodynamic principles of heat transmission and fluid mechanics. (Mouzinho et al., 2006).

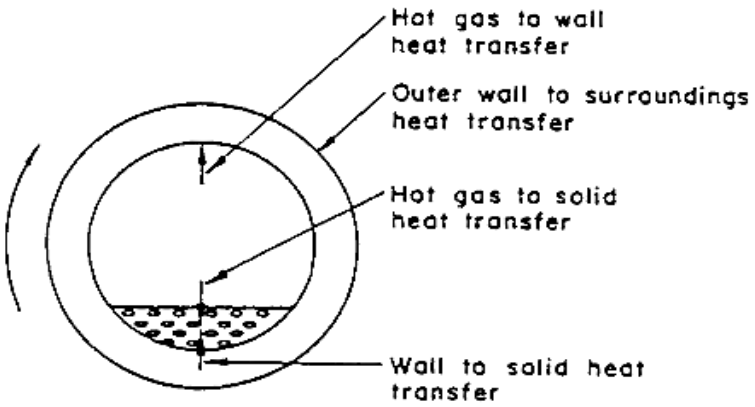

Figure 2.3: Schematic illustration of the heat transport channels in the kiln (Ghoshdastidar et al., 2002)

2.1.3 Mathematical Modeling for Rotary Kiln Temperature

According to Csernyei & Straatman, 2016, the primary source of heat in the plant is the rotary cement kiln, and researchers have conducted studies on it using one-dimensional mathematical models and three-dimensional CFD simulations. Mujumdar & Ranade, 2006 demonstrates a one-dimensional framework for predicting essential processes in cement kiln solid beds using a pseudo-homogeneous approximation, modifying bed

height and melt formation, and solving energy balance including convective, conductive, and radiative heat transfer using a quasi-steady state approach. The model is dynamically simulated and evaluated using data collected during the cement production process. The simulation results of the model correspond to the actual conditions. (Sun et al., 2020) These models can be efficient tools for the optimization and operation of the kiln by studying the effects of key control variables such as kiln slope, speed and production rate (Georgallis et al., 2005).

Agrawal & Ghoshdastidar, 2018 used a standalone CFD model to investigate convective heat transfer from gas to wall and solid in a nonrotating kiln. The finite-difference method is used to investigate the uneven heat conduction in the refractory wall, which is alternately heated and cooled throughout each round. A steady-state mathematical representation of rotary cement kilns is developed based on principal physical and chemical operations. The temperatures of the gas, block, and wall surface zones are determined using the zonal methodology, while the total radiative exchange areas of the thermocouple with all other zones in the kiln are computed using the Monte Carlo method. (S2214157X21000010, n.d.)

2.1.4 Temperature Measurement in Rotary Kilns

Production-related parameters have to be filtered before being used for dynamic modeling or control. Non-uniform friction and system wear are examples of inherent nonlinear dynamics that cannot be captured by first principle models. (Hasfjord, 2014) Temperature is one of the most essential factors describing any thermodynamic system and is of vital significance in the cement pyro process from a safety, control, and efficiency perspective. The acoustical pyrometer allows accurate and dependable gas temperature readings for use in combustion and emission control systems. (Kychakoff et al., 2005).

Temperature can be measured using a wide variety of techniques, including thermoelectricity, temperature-dependent variation in electrical conductor resistance, fluorescence, and spectral properties. (Childs et al., 2000) The precise and real-time measurement of temperature in the burning zone is critical for producing high-quality clinker with low pollutant emissions. Touch temperature measurement is problematic; hence the temperature is measured using a pyrometer. (Matias et al., 2013).

The dependability of both the refractory and thermal insulation layers is crucial for ensuring that cement kilns operate well over time. Nonetheless, in the research of rotary cement kilns, the use of shell scanners is regarded as the most appropriate because standard IR thermometers are incapable of performing temperature monitoring and IR imaging radiometers are too expensive (Torgunakov & Vavilov, 2003).

The rotary kiln shell temperature monitoring system improves as technology advances. The thermocouple and radiation pyrometer are popular monitoring devices. These instruments' measured readings are imprecise and do not exactly reflect the temperature of the revolving kiln shell (T. Liu et al., 2017) Among the several temperature detectors available, thermocouples are popular because they are tiny, inexpensive, and have a quick response time (Glavatskih, 2004).

2.1.5 Significance of Kiln System Monitoring

The occurrence of a fault in a rotary kiln system can cause considerable economic damage and even destruction of the total drive system (Kadri & Mouss, 2017) The simple bearings inside the retaining rollers allow the rotary kiln to function at a steady pace with tremendous loads of up to 15,000–20,000 kN (Zheng et al., 2016) as shown in **Figure 2.4** below.

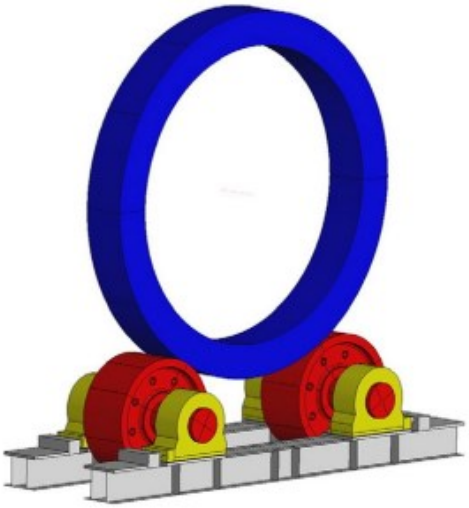

Figure 2.4: Supporting roller station comprising of tire, rollers and bearings (Alhajjaji et al., 2016)

Bearings can turn less forgiving at lower speeds than at higher operating rates. A solid awareness of varied operating and environmental conditions, coupled with possible failure modes, aids the designer in designing durable bearings (Singhal, 2008). Highly advanced methods of signal processing, together with automatic detection of problems, provide dependable condition monitoring even when long periods of continuous operation are required (Juuso & Lahdelma, 2017).

Monitoring and measurement of rotary kiln's axis have the great significance on adjusting technical process reasonably, avoiding the roller bearing overheat, lessening the kiln shell stress and protecting the shell (Hu & Guo, 2016)

2.1.6. Data Processing Techniques in Industrial Applications

A system of processing and collecting data consists of both hardware and software. A hardware system creates point clouds or volumetric data by interacting with an object's surface or volume via well-known mechanisms or phenomena. A software system turns raw point clouds or volumetric data into a virtual representation of the object, containing surfaces and features (Bia & Wang, 2010).

In data analysis, items with certain qualities are considered. Objects can be people, equipment, products, time series, sensor signals, process states, and so on. The particular values of the properties are what will be evaluated. The basic goal is to expose the structure (information) of these data (Noll, 2020).

2.2. State Estimation and Kalman Filtering

2.2.1 Introduction to State Estimation

State estimation is one of the most commonly used approaches for finding likely values of a system state using measurements (Jin et al., 2021) State estimation is a critical function in energy management systems for developing a network real-time model (Monticelli, 2000) Some states in a system are difficult to measure; otherwise, certain findings are inaccurate due to sensor uncertainty (Jin et al., 2021).

The state estimation solution is iterative using the Kalman filter estimates x_k at time k, initial estimate of x_0, a series of measurements (z_1, z_2, …, z_k), and system information (F, B, H, Q, R) (Kim & Bang, 2019) In developing an indirect measuring model for an electro thermal furnace and implementing it in a reconfigurable architecture, Mouzinho et al., 2006 used the Kalman filter algorithm to generate an optimal estimate of the temperatures within the combustion chamber while reducing uncertainty in temperature prediction. In contrast with typical frequency-based filters, the Kalman algorithm is a time domain filter that iteratively estimates process states using input from both an evolving system model and observed measurements (Hasfjord, 2014) In practice, the actual values of estimation covariance Q and R are unknown a priori, therefore their time changes are typically neglected. This results in estimating errors, which can diverge the Kalman filter operation (Mosallaei et al., n.d.).

The Kalman filter, which remains one of today's most used data fusion techniques, provides a modest computing load and sufficient recursive advantages. It is regarded as an optimum estimator in one-dimensional linear systems with Gaussian error statistics (Claude et al., 2017).

2.2.2 Kalman Filtering Theory

A recursive linear estimator such as the Kalman Filter progressively derives an estimate for an evolving valued state that changes over time, in line with regular evaluations of this state (Babu, 2018) The measured results are expected to be impacted by inaccuracies arising from randomized zero-mean white Gaussian noise (Wang & Leng, 2018) Consider the Kalman filter system model below;

$$\begin{cases} \boldsymbol{x_{k+1}} = \boldsymbol{F_{x_k}} + \boldsymbol{w_k} \\ \boldsymbol{y_k} = \boldsymbol{H_{x_k}} + \boldsymbol{v_k} \end{cases} \tag{2.4}$$

Given k is the time step, wk and vk are the zero-mean process noise and measurement noise with covariance Q and R respectively while $\mathbf{x_k}$ is the state, $\mathbf{y_k}$ is the measurement, F and H are the state transition and measurement matrices (Simon, 2010)

The filter in discussion, which has long been one of the most popular signal recovery methods in classical systems, is now coupled to the stochastic master equations of linear quantum mechanical systems. Prediction approaches such as the Kalman filter series, EKF, UKF, CKF, and particle filtering have resulted in many published study findings. They are widely employed in various detecting, tracking, and control systems (Jin et al., 2021) The Kalman filter and extended Kalman filter are effective in minimizing forecast error by properly characterizing the initial state of a forecast using available monitoring resources. However, they require computer systems processing of the time-dependent error covariance matrix (Farrell & Ioannou, 2001).

2.2.3 Kalman Filter variants

The Kalman filter being a state estimation technique ideally blends system information and measurements to reduce the mean squared error of estimated states. While KF was initially designed for linear systems, various extensions of it, such as the extended Kalman filter (EKF), unscented Kalman filter (UKF), cubature Kalman filter (CKF), etc., have been proposed for nonlinear systems (Shi & Moura, 2024).

2.2.3.1 Extended Kalman Filter (EKF)

An extended Kalman filter is used to predict the fault-related parameters, and a threshold-based decision algorithm processes the parameter forecasts to detect probable faults (Huang et al., 2009) The Extended Kalman filter (EKF) is a suboptimal way to solving the problem using linear filters. The EKF implements a Kalman filter for a system dynamics that arises from the linearization of the initial non-linear filter dynamics around the previous state estimates (Ribeiro, 2004) While studying the non-linear cell behavior, Campestrini et al., 2016, rarely used the LKF in. The KF is then applied to batteries after linearizing the system and measurement matrices in the actual state using the first-order Taylor approximation of the differential equations.

To include non-linear behavior, we assume that the state-space equation and measurement equation have the form;

$$\mathbf{x}_{k+1} = \boldsymbol{f}\ (\mathbf{x}_k, \mathbf{u}_k) + \mathbf{w}_k \tag{2.5}$$

$$\mathbf{y}_k = \mathbf{g}\ (\mathbf{x}_k, \mathbf{u}_k) + \mathbf{v}_k \tag{2.6}$$

with two well-defined and differentiable functions f and g. (Campestrini et al., 2016).

2.2.3.2 Continuous Kalman Filter

Consider a dynamical system whose state is defined by a linear, vector differential equation. The process and measurement models are depicted as follows:

$$\text{Process model: } \boldsymbol{x} = \boldsymbol{F}\boldsymbol{x} + \boldsymbol{G}\boldsymbol{w} \tag{2.7}$$

$$\text{Measurement model: } \boldsymbol{z} = \boldsymbol{H}\boldsymbol{x} + \boldsymbol{v} \tag{2.8}$$

Where the vectors $\mathbf{u}(t)$ and $\mathbf{v}(t)$ are both white noise sequences with zero means and mutually independent (Jwo & Biswal, 2023).

One issue with implementing the Kalman filter for state identification and forecasting is that the matrix changes necessary are excessively expensive computationally (Farrell & Ioannou, 2001).

2.2.3.3 Unscented Kalman Filter (UKF)

With processes identical to the EKF, the UKF often provides superior efficiency and reduced complexity due to the sampling technique, and it avoids the divergence of errors common in the EKF (Gupta et al., 2021) This technique is used to linearize a nonlinear function of a random variable by employing a linear regression between n points taken from the random variable's prior distribution (Terejanu, 2011).

2.2.3.4 Ensemble Kalman Filter (EnKF)

The ensemble Kalman filter (EnKF) is a computational approach for doing approximate inference on state-space models. Most applications use state vectors, which are large geographical fields recorded progressively over time. The EnKF, like the Kalman filter, expresses the state distribution as an ensemble of draws from that distribution (Katzfuss et al., 2016) In his study, Liang et al., 2024 suggested an updated adaptive EnKF method to increase the smoothness and accuracy of the filtering process. Instead of the standard Gaussian distribution, this technique used a Laplace distribution to create the system state vector and observation vector ensembles, which enhanced robustness against non-Gaussian noise

2.2.4 Applications of Kalman Filtering in Thermal Systems

In general, a system that we work with using a Kalman filter is prone to random disturbance (process noise) as it evolves in accordance with a motion equation. Our goal is to generate the best approximation of this system's state at a given instant using data acquired at many observation points (measurement sites) (Daum, 2021) In the field of mobile robotics and sensor networks, the necessity for flexible and resilient filtering algorithms is increasing with the expanding use of vast networks of cheap mobile agents with simple sensors (Karasalo & Hu, 2011) Given the increasing demand for highly precise temperature measurement and constricted onboard resources in the spacecraft's hostile thermal environment, producing temperature data with high precision is crucial in spaceflight operations. However, the question of how to collect data is critical. The Kalman filtering method is one of the ways for getting this data with limited resources (Zhang et al., 2022).

It is commonly accepted that Numerical Weather Prediction (NWP) models make consistent errors in forecasting near-surface weather conditions. This is related not just to errors in physical parameterization, but also to the models' inability to appropriately capture sub-grid events. A straightforward approach to the aforementioned issues is the application of Kalman filtering (Galanis & Anadranistakis, 2002) One challenge with implementing the Kalman filter for state identification for forecasts is that the matrix changes required are overly costly computationally (Farrell & Ioannou, 2001).

Knowledge of the immediate junction temperature is crucial for successful power converter health management, allowing power semiconductors to operate safely in all operating conditions. Junction temperature measurements are obtained using an online measurement of the on-state voltage at high current and processed by a Kalman filter,

which uses a predict-correct process to offer an adaptive estimate of the junction temperature (Eleffendi & Johnson, 2016).

Numerical weather prediction (NWP) models typically demonstrate systematic inaccuracies in forecasting near-surface weather parameters due to a variety of causes, including low model topography resolution or insufficient physical parameterizations. During his work, (Lai et al., 2019) an examination of 12 synoptic stations in Portugal was conducted, and differences between 2 m-temperature data and forecasts given by the European Centre for Medium-Range Weather Forecasts (ECMWF) were identified. Systematic mistakes vary significantly by geographical location, time of day, and year. The Kalman Filter theory offers an appropriate technique for correcting systematic mistakes of this type, resulting in improved model forecasts.

Massano et al., 2020 developed a grey-box model to estimate thermal changes in buildings using the Unscented Kalman Filter and thermal network modeling. He says that houses account for around 40% of primary energy demand. Such energy data can be used to train data-driven models that learn about building thermal properties and predict the evolution of indoor temperatures.

Kalman Filter models can effectively predict human core body temperature using skin temperature, heat flow, and heart rate data. The Kalman filter approach yields similarly accurate estimations of core body temperature when just two of these three input variables are known (Welles et al., 2018). The main benefits of using a Kalman filter include its ability to adapt to environmental changes and account for errors caused by process noise (Ozceylan et al., 2020). Kalman filtering can be utilized to considerably reduce or smooth the noise that exists in the output of a sensor data collection in which the errors in

measurement form a Gaussian or normal distribution around the genuine value of the parameter being tracked (Smythe, 2021).

Due to their capacity to undertake state estimation of nonlinear systems, EKFs have found substantial application in estimating the rotor position and speed in synchronous motor drives. (Auger et al., 2013).

Mironova et al., 2020 explored the creation of an observer for a nonlinear thermoelectric system containing a Peltier cell using an Extended Kalman Filter (EKF). The EKF was created to estimate temperatures on both the cold and warm sides of the computer, allowing for sensor-free temperature control on the cold side without relying on direct readings. Experimental validation on a customized test bench showed that the EKF delivered highly accurate estimation results, even throughout the milling operation.

Soh & Cho, 2020 combined noise reduction technique incorporating wavelet transform and Kalman smoothing yielded higher accuracy than Kalman filtering alone. When applied to ocean temperature sensor measurements, the method increased the accuracy and stability of the sensor results.

Sajid et al., 2023 unveiled an enhanced dual Extended Kalman Filter (EKF) technique for predicting and tracking the temperature of lithium-ion battery cells. The method used basic but effective dynamic and measurement empirical fit models, allowing for the simultaneous determination of temperature and charge. The proposed dual estimator significantly improved temperature state estimation accuracy by taking into account changes in the state of charge.

2.3 Validation and Performance Evaluation

2.3.1 Model validation

Precise system modeling and identification, as well as the analysis of system noise and the identification of fault-related components, result in a reliable fault estimation.-state (Huang et al., 2009). Phasor measurement was previously used for sub-system model validation, permitting a full comparison of model simulation and recorded dynamics and facilitating the detection of problematic model components (Huang et al., 2009)

Prior to simulating the rotating kiln, the suggested model is evaluated using the steady-state operation to replicate the obtained findings. (*implementation of a mathematical modelling*, 2020)

de Carvalho Blanc et al., 2017, validated the suggested EKF technique for estimating the IMU-camera transformation when ground truth is provided and conducted a series of simulated experiments. In the simulation scenario, an IMU-camera rig moved in front of a calibration target with 25 known features. Two models of visual measurements for Kalman-based filters were proposed by Ligorio & Sabatini, 2013, with the DLT-based EKF being more accurate and less robust against visual feature loss. The IMU-based EKF achieved orientation RMSEs of 1.6°, while the error-driven EKF achieved 1° and 3.5mm.

Ligorio & Sabatini, 2013 created a learning module based on ANN to assess the level of error in current readings and update R in the Kalman filter correctly. Experiments revealed that the Kalman filter with the learning module outperformed the regular Kalman filter algorithm (4.41%-11.19%) in terms of the root mean squared error measure.

To examine the performance of predicting building energy use using distinct algorithms and models, Yang & Mao, 2023 used , mean square error (MSE), root mean square

deviation (RMSE), and mean absolute error (MAE) are used to evaluate the efficacy of various models.

2.3.2 Evaluation Criteria using performance metrics

Several measures relevant to measuring various elements of an estimating algorithm's performance are introduced and justified (Introduction, 2006). A variety of performance metrics can be used to evaluate model performance. In this study, performance indicators such as mean absolute error (MAE), root mean square error (RMSE), and coefficient of determination R2 were used to evaluate model outcomes (Benrhmach et al., 2020) . MAE is a statistic that is less sensitive to extremes in projected values than RMSE, and the lower the value, the better the performance. (Hadeed et al., 2020).

2.4 Summary and Research Gap

Disruptions and uncertainties are unavoidable phenomena in industrial control systems, which frequently have negative consequences on their performance. (H. Sun et al., 2022) The Kalman filter is a state estimator that reduces variance in linear dynamic systems with Gaussian noise. Even with non-Gaussian noise, the Kalman filter is the best linear estimator (Simon, 2010) The Kalman filter is a linear estimator that iteratively computes the estimate for a continuously valued state (Babu, 2018) As a linear minimum variance estimation-based method, it may estimate the true state of the system from data that has been distorted by measurement and process issues (Cui et al., 2020)

The Kalman filter is an important tool in many domains, including orbit calculation, target tracking, navigation, integrated navigation, dynamic positioning, sensor data fusion, microeconomics, and digital image processing, particularly pattern identification and picture segmentation (Li et al., 2016) Its application in the specific context of enhancing the accuracy of kiln roller bearing temperature measurements in cement

production has not been extensively explored. This research aims to fill this gap by developing a Kalman Filter-based Algorithm tailored to this application.

CHAPTER THREE : METHODOLOGY

3.1 Derivation of the Mathematical Model

The study involves principles of bearing temperature measurements and identifies common parameters influencing these measurements with a focus on kiln bearings. Observational studies have been conducted to collect temperature data and related parameters such as load, speed, and ambient temperature. These parameters characterize the current state of the system.

3.1.1 Mass Conservation Equation

To derive the mass conservation equation of a cement rotary kiln, it is suggested to consider the system as a control volume where mass enters, moves through, and exits. It is mentioned that the kiln can be divided into four segments for the firing system: drying, preheating, calcining, and sintering (or clinkering).

It is assumed that the process is in a steady-state, meaning that the mass flow rate is constant over time. The general form of the mass conservation equation, also known as the continuity equation, is presented as

$$\frac{d}{dx}(\rho A u_s) = \dot{m}_{in} - \dot{m}_{out} \tag{3.1}$$

Where; ρ = density of the material (kg/m³), A = cross-sectional area of the kiln segment (m²), u_s = velocity of the material through the kiln segment (m/s), $\dot{m}_{In}$ = mass flow rate of the input material (kg/s), $\dot{m}_{Outc}$= mass flow rate of the discharged material (kg/s), $\frac{d}{dx}$ = denotes the derivative along the length of the kiln.

Assume that the cross-sectional area A of the kiln is constant and that there are no internal sources or sinks of mass. Consequently, it is stated that the mass conservation equation (3, 1) for a differential segment of the kiln could be simplified to;

$$\frac{d}{dx}(\rho u_s) = 0 \tag{3.2}$$

From (3, 2), It is noted that by integrating this over the length of the kiln, considering the four segments, and incorporating the mass flow rates at the input and output, a more comprehensive equation that accounts for the mass conservation in each segment is obtained as below;

$$\sum_{i=1}^{4} \int L_i \frac{d}{dx}(\rho_i u_i) dx = \dot{m}_{In} - \dot{m}_{Out} \tag{3.3}$$

Where L_i, ρ_i, and v_i represent the length, density, and velocity of the material in each of the four segments (i = 1, 2, 3, 4), respectively. It is noted that the sum over the four segments accounted for the entire length of the kiln.

It is stated that (3, 3) represents the conservation of mass along the kiln, assuming no loss of material to the environment (a closed system), and it is simplified to:

$$\dot{m}_{In} = \dot{m}_{Out} \tag{3.4}$$

It is emphasized that evaluating these parameters segment-by-segment is essential to accurately modeling the mass flow through the kiln because the density and velocity of the material could vary across the different segments due to thermal and chemical reactions, such as moisture evaporation in the drying segment and decomposition of limestone in the calcining segment as shown in (3, 5).

$$\begin{cases} \frac{d\rho_1}{dt} = \frac{1}{L_1}(\dot{m}\mathrm{In} - \rho_1 u_s) \\ \frac{d\rho_2}{dt} = \frac{1}{L_2}(\rho_1 u_s - \rho_2 u_s) \\ \frac{d\rho_3}{dt} = \frac{1}{L_3}(\rho_2 u_s - \rho_3 u_s) \\ \frac{d\rho_4}{dt} = \frac{1}{L_4}(\rho_3 u_s - \rho_4 u_s) \end{cases} \tag{3.5}$$

3.1.2 Material Energy Conservation Equation

This is a heat balance equation for a differential element of the material, taking into account convection with surrounding gases, conduction from nearby sections, heat

generation or absorption from processes, and heat loss to the environment for a differential portion of the material.

It is stated that the efficiency of the kiln operation depends on maintaining a balance between the input raw materials and the output, adjusting the process parameters to minimize losses, and efficiently transforming the raw feed into high-quality clinker. The basic form of the material energy conservation equation for a kiln firing system is then expressed as:

$$\mathbf{Q_{in} = Q_{out} + Q_{loss} + \Delta Q} \quad (3.6)$$

Where; Q_{in}represents the total energy input into the system, Q_{out} represents the total energy output from the system including the sensible heat in the product and exhaust gases, Q_{loss} accounts for energy losses from the system including losses through the kiln walls and any other unaccounted for losses, ΔQ represents the net change in enthalpy of the materials being processed, accounting for any chemical or phase changes.

Also Considering parameters;

Where $\boldsymbol{c_{ps}}$: Specific heat capacity of the solid material (J/kg·K), $\boldsymbol{c_{pg}}$: Specific heat capacity of the gas (J/kg·K), $\boldsymbol{T_{s,i}}$: Temperature of the material into i th segment (K), $\boldsymbol{T_{g,i}}$**:** Gas temperature into the ith segment (K), $\boldsymbol{k_{g,s}}$: Overall heat transfer coefficient between the gas and solid (W/m²·K), $\boldsymbol{k_l}$: Heat loss coefficient MJ / (m.k.h), $\boldsymbol{\Delta H_f}$ **:** Enthalpy change of conversion, MJ / Kg, $\boldsymbol{Q_{s,in}}$ **:** Rate of heat input into the segment (W).

According to **Fourier's Law of Heat Conduction**, the heat transmission rate through a material is proportional to the negative gradient in temperature and the area perpendicular to the gradient of the surface through which the heat flows. The term $c_{ps}Q_{in}(T_{S,in-}\ T_{s,1})$, models the heat conducted from one section of the material to the next.

Newton's Law of Cooling states that the rate of loss of heat from a body is correlated to the temperature differential between the body and the environment, which can be expressed by the term $k_{gs,1}L_1\left(T_{g,1} - T_{s,1}\right)$ which models the heat exchange between the solid material and the surrounding gas.

$k_l L_1 T_{s,1}$ Models heat loss, through radiation to the environment based on the **Stefan-Boltzmann Law** as shown in (3, 5) below;

$$\begin{cases} \frac{dT_{s,1}}{dx} = \frac{1}{c_{ps}(m_{s,1}L_1)}[c_{ps}Q_{in}(T_{S,in-}T_{s,1}) + k_{gs,1}L_1\left(T_{g,1} - T_{s,1}\right) - k_l L_1 T_{s,1}] \\ \frac{dT_{s,2}}{dx} = \frac{1}{c_{ps}(m_{s,2}L_2)}[c_{ps}m_{s,1}u_s(T_{s,1} - T_{s,2}) + k_{gs,2}L_2\left(T_{g,2} - T_{s,2}\right) - k_l L_2 T_{s,2}] \\ \frac{dT_{s,3}}{dx} = \frac{1}{c_{ps}(m_{s,3}L_3)}[c_{ps}m_{s,2}u_s(T_{S,2-}T_{s,3}) + k_{gs,3}L_3\left(T_{g,3} - T_{s,3}\right) - k_l L_3 T_{s,3}] \\ \frac{dT_{s,4}}{dx} = \frac{1}{c_{ps}(m_{s,4}L_4)}[c_{ps}m_{s,3}u_s(T_{S,3-}T_{s,4}) + k_{gs,4}L_4\left(T_{g,4} - T_{s,4}\right) - k_l L_4 T_{s,4}] \end{cases} \quad (3.5)$$

3.1.3 Gas Conservation Equation

It is explained that fuel consumption, clinker quality, and emissions management are all impacted by the gas conservation equation in the kiln, which have to be understood and optimized for effective kiln operation. It is also noted that the composition of the input materials, such as raw meal and coal, as well as the thermodynamics of the gas phase, need to be thoroughly understood in order to effectively calculate the gas conservation equation in a cement rotary kiln as presented in (3, 6).

$$\begin{cases} \frac{dT_{g,1}}{dt} = \frac{1}{c_{p,g}m_g L_1}\left[c_{p,g}\rho_{g0}Q_{a,o}\left(T_{g,2} - T_{g,1}\right) - k_{g,s}L_1\left(T_{g,1} - T_{s,1}\right)\right] \\ \frac{dT_{g,2}}{dt} = \frac{1}{c_{p,g}m_g L_2}\left[c_{p,g}\rho_{g0}Q_{a,o}\left(T_{g,3} - T_{g,2}\right) - k_{g,s}L_2\left(T_{g,2} - T_{s,2}\right)\right] \\ \frac{dT_{g,3}}{dt} = \frac{1}{c_{p,g}m_g L_3}\left[c_{p,g}\rho_{g0}Q_{a,o}\left(\rho_{ao}T_{g,4} - \rho_{go}T_{g,3}\right) - k_{g,s}L_3\left(T_{g,3} - T_{s,3}\right) - Q_f\Delta H_f\right] \\ \frac{dT_{g,4}}{dt} = \frac{1}{c_{p,g}m_g L_4}\left[c_{p,g}\rho_{a0}Q_{a,o}\left(T_{a,in} - T_{g,4}\right) - k_{g,s}L_4\left(T_{g,4} - T_{s,4}\right)\right] \end{cases} \quad (3.6)$$

It is clarified that under steady-state conditions, $m_{s,in} \times u_s = Q_{s,in}$, becomes a constant parameter equal to the steady-state value data $m_s = \frac{Q_{s,in}}{u_s}$. Thus, the material mass density equation has been ignored for purposes of simplifying the model. It is also mentioned

that the relationship between the amount of coal injected and the amount of entering air is directly tied to the oxygen content equation of the kiln exhaust gas. Additionally, this relationship is removed because pulverized coal is instantly burnt and consumed in the firing zone.

The equation of state (3.7) is thus found by combining the (3.5) and (3.6) deciding on the state vector x in eight dimensions, x = $[T_{s1}, T_{s2}, T_{s3}, T_{s4}, T_{g1}, T_{g2}, T_{g3}, T_{g4}]^{T}$ and the control input being u = $[Q_{s,in}, Q_f, Q_{ao,} T_{s,in}, T_{a,in}]$

$$\begin{cases} \frac{dx_1}{dt} = \frac{u_1(u_4 - x_1)}{ms_1 L_1} + \frac{k_{gs,1}(x_5 - x_1)}{c_{ps} m_{s,1}} - \frac{k_l x_1}{C_{ps} m_{s,1}} \\ \frac{dx_2}{dt} = \frac{u_1(x_1 - x_2)}{ms_2 L_2} + \frac{k_{gs,2}(x_6 - x_2)}{c_{ps} m_{s,2}} - \frac{k_l x_2}{C_{ps} m_{s,2}} \\ \frac{dx_3}{dt} = \frac{u_1(x_2 - x_3)}{ms_3 L_3} + \frac{k_{gs3}(x_7 - x_3)}{c_{ps} m_{s3}} - \frac{k_l x_3}{C_{ps} m_{s3}} \\ \frac{dx_3}{dt} = \frac{u_1(x_2 - x_3)}{ms_3 L_3} + \frac{k_{gs3}(x_7 - x_3)}{c_{ps} m_{s3}} - \frac{k_l x_3}{C_{ps} m_{s3}} \\ \frac{dx_4}{dt} = \frac{u_1(x_3 - x_4)}{ms_4 L_4} + \frac{k_{gs,4}(x_8 - x_4)}{c_{ps} m_{s,4}} - \frac{k_l x_4}{C_{ps} m_{s,4}} \\ \frac{dx_5}{dt} = \frac{\rho_{go} u_3(x_6 - x_5)}{m_g L_1} + \frac{k_{gs,1}(x_5 - x_1)}{c_{pg} m_g} \\ \frac{dx_6}{dt} = \frac{\rho_{go} u_3(x_7 - x_6)}{m_g L_2} + \frac{k_{gs,2}(x_6 - x_2)}{c_{pg} m_g} \\ \frac{dx_7}{dt} = \frac{u_3(\rho_{ao} x_3 - \rho_{go} x_7)}{m_g L_3} - \frac{k_{gs,3}(x_7 - x_3)}{c_{pg} m_g} - \frac{u_2 \Delta H_f}{C_{pg} m_g L_3} \\ \frac{dx_8}{dt} = \frac{\rho_{go} u_3(x_5 - x_8)}{m_g L_4} + \frac{k_{gs,4}(x_8 - x_4)}{c_{pg} m_g} \end{cases} \quad (3.7)$$

This equation is expressed as;

$$\dot{x} = f(x, u, t) \quad (3.8)$$

It is stated that given the system noise being w, the equation of state for the cement rotary kiln would be:

$$\dot{x} = f(x, u, t) + w \quad (3.9)$$

Where system noise w = $[w_1, w_2, w_3, w_4, w_5, w_6, w_7, w_8]^{T}$

3.2 Developing the Kalman Based Filter Algorithm

3.2.1 System Model Definition

State Variables: These encompass physical parameters characterizing the system's current state, such as the temperature of the kiln roller bearings and their rate of temperature change.

Process Model: This describes the gradual evolution of the state variables during temperature monitoring. To accommodate modeling errors and unforeseen circumstances, a basic model assumes linear dynamics, where the next state is a function of the current state plus some process noise. The process model is expressed as:

$$\boldsymbol{x_k = Ax_k - 1 + Bu_k + w_k} \tag{3.10}$$

Where, x_k is the state vector at time k, A is the state transition matrix, B is the control-input matrix (if applicable), u_k is the control vector, w_k is the process noise, modeled as a Gaussian with zero mean and covariance Q.

Observation Model: It is mentioned that with additional measurement noise, temperature readings directly related to one of the state variables, such as the kiln bearing temperature. The observation model is described as:

$$\boldsymbol{z_k = Hx_k + v_k} \tag{3.11}$$

Where z_k is the measurement vector at time k, H is the observation matrix that maps the true state space to the observed space, and v_k is the measurement noise, which can also be represented as a Gaussian with zero mean and covariance R.

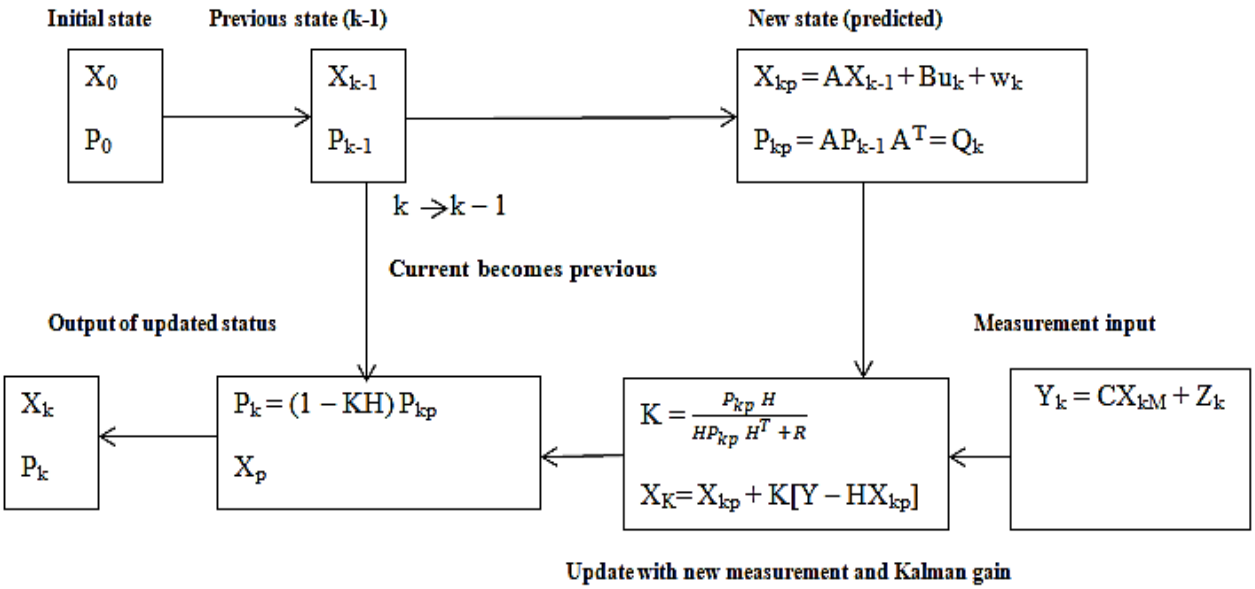

Figure 3.1: Illustration of the Kalman filter framework

Given that X is state matrix, P = Process covariance matrix, K = Kalman Gain, Q = Process Noise Covariance Matrix, I = Identity Matrix, R = Sensor Noise covariance matrix, Y = Measurement of the state, u = Control Variable Matrix, w = Predicted state noise matrix

3.2.2. Extended Kalman Filter

The Extended Kalman Filter (EKF), an iterative technique for state prediction in nonlinear systems, is utilized as a buildup by linearizing the system dynamics and observation models around the current estimate with Jacobians. Adapting the standard Kalman filter equations to the described nonlinear dynamics yields the EKF for the given system as shown in equation (3.12)

Nonlinear State-Space Model

The generic nonlinear state-space model is;

$$\begin{cases} \boldsymbol{x_{k+1}} = f(\boldsymbol{x_k}, \boldsymbol{u_k}) + \boldsymbol{w_k} \\ \boldsymbol{z_k} = \boldsymbol{h}(\boldsymbol{x_k}) + \boldsymbol{v_k} \end{cases} \tag{3.12}$$

Where; x_k: State vector at time k, u_k: Control input vector at time k, z_k: Measurement vector at time k, w_k: Process noise ($w_k \sim N(0, Q_k)$), v_k: Measurement noise ($v_k \sim N(0, R_k)$).

In this case, $f(x_k, u_k)$ is the state transition function defined by the system dynamics; $\frac{dy}{dt} = f(x, u)$ while $h(x_k)$ maps the state x_k to measurements.

Initializing the Kalman Filter

This includes establishing the initial state estimate and the initial estimate covariance matrix. These act as best guesses before any measurements are processed.

Predict and Update Cycles

It is stated that the Kalman Filter operates in two steps: predict and update. The prediction step uses the process model to foresee the next state and assess its uncertainty. In the update process, the latest measurement data is used to adjust the forecast and reduce its uncertainty.

The equations for these steps are outlined as follows:

Prediction:

Predicted state estimate: $$\hat{\boldsymbol{x}}_{\mathbf{k|k-1}} = \boldsymbol{f}(\hat{\boldsymbol{x}}_{\boldsymbol{k-1|k-1}}, \boldsymbol{u_k}) \quad (3.13)$$

Predicted covariance estimate: $$\boldsymbol{P_{k|k-1}} = \boldsymbol{F P_{k-1|k-1} F^T} + \boldsymbol{Q_k} \quad (3.14)$$

Where; $F_k = \frac{\partial f}{\partial x}$ is the Jacobian of $f(x, u)$ with respect to the system state.

Update:

The Kalman gain: $$\boldsymbol{K_k} = \boldsymbol{P_{k|k-1} H^T} (\mathbf{H} \boldsymbol{P_{k|k-1} H^T} + \boldsymbol{R_k})^{-1} \quad (3.15)$$

Updated state estimate: $$\hat{\boldsymbol{x}}_{\boldsymbol{k|k}} = \hat{\boldsymbol{x}}_{\boldsymbol{k|k-1}} + \boldsymbol{K_k}(\boldsymbol{z_k} - \boldsymbol{H}\hat{\boldsymbol{x}}_{\boldsymbol{k|k-1}}) \quad (3.16)$$

Updated covariance estimate: $$\boldsymbol{P_{k|k}} = (\boldsymbol{I} - \boldsymbol{K_k H}) \boldsymbol{P_{k|k-1}} \quad (3.17)$$

Where;

$H_k = \frac{\partial H}{\partial x}$ is the Jacobian of $H(x)$ with respect to the system state

Iteration: The predict-update cycle recurs with each new measurement, constantly improving the state estimate and its uncertainty.

Anomaly Detection

The Mahalanobis distance-based approach is used to look for statistical anomalies by comparing the given measurements to the predictions.

Residual (Innovation);

$$\mathbf{y_k = z_k - Hx_{k|k-1}} \tag{3.18}$$

Where; y_k: Measurement residual or innovation.

Mahalanobis Distance;

$$\mathbf{d_k} = \sqrt{\boldsymbol{y_k^T S_k^{-1} y_k}} \tag{3.19}$$

Where: d_k: Mahalanobis distance (used to identify anomalies), $S_k = HP_{k|k-1} H^T + R$: Innovation covariance matrix, an anomaly is detected if $d_k >$ threshold.

3.2.3. Extended Kalman Filter Framework

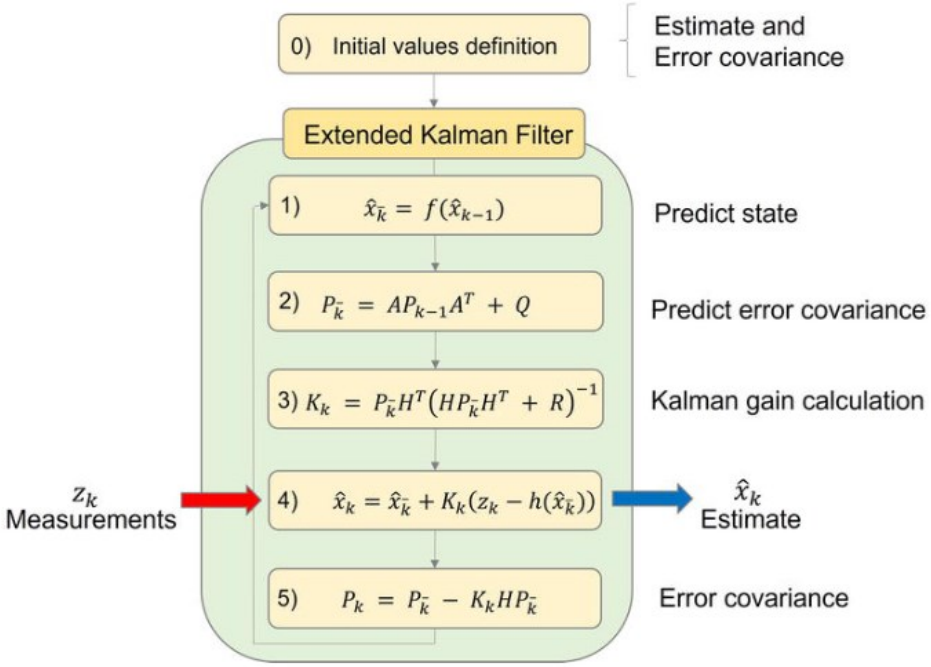

Figure 3.2: Representation of the extended Kalman filter algorithm

The Kalman Filter algorithm suited to the unique needs of temperature measurement for kiln roller bearings has been developed. This includes defining the state vector (bearing temperature), observation model (sensor readings), and noise covariance (process and measurement noise). The Kalman Filter algorithm is then applied to the noisy temperature readings from the sensors attached to the kiln roller bearings and generates estimates of the true bearing temperatures. The algorithm is coded using Python programming language and software environment.

3.3 Validation of the Proposed Algorithm

Having developed the model, it is tested with actual data from the kiln roller bearing temperature measurements. The model's parameters, such as the process noise covariance Q and measurement noise covariance R, are tuned based on the filter's performance using ground truth data. Temperature sensors with known characteristics, including their accuracy, precision, and response time are used for the kiln operating conditions.

The efficacy of the model is then tested by comparing its estimations in immediate processing and its ability to enhance the temperature measurement accuracy.

3.3.1 Data Collection

A comprehensive dataset with kiln in normal operating conditions is collected and documented which includes the HPR temperature from the kiln station roller bearings and the CCR reading. While using a fluke hand pyrometer, bearing temperature measurement are taken for each bearing, at each kiln roller station. These readings are taken at 30 minute time intervals starting from 0100hrs to 1400hrs. Considering the same time interval, records from control room are also trended and recorded for the different bearings for comparison purposes. A set of measurement instruments, such as pyrometers and kiln bearing temperature thermocouples, are used to demonstrate their rationale for their selection. After data has been collected, Ms Excel is used to graphically present the results.

3.3.2 Data Analysis

The data is evaluated to compare the accuracy of the temperature measurements obtained. Statistical approaches such as root mean square error are employed to assess measurement accuracy.

$$\mathbf{RMSE} = \sqrt{\frac{1}{N}\sum_{i=1}^{N}(T_{true,i} - T_{measured,i})^2} \quad (3.9)$$

Where $T_{true,\,i}$ = ground truth temperature, $T_{measured,\,i}$ = Control room measured temperature

A report on the findings, emphasizing the impact of the Kalman Filter on enhancing the accuracy of kiln roller bearing temperature measurements, as well as providing recommendations for practical applications in cement production facilities is then generated.

CHAPTER FOUR: RESULTS AND DISCUSSION

4.1 Mathematical Modeling of Kiln Temperature Dynamics

The intention is to model heat transport in a cement rotational kiln, specifically how it influences the temperature of roller bearings. The kiln is divided into four segments: decomposition zone, transitional zone, burning zone and the cooling zone. The model considers both conductive and convective heat transfer modes.

4.1.1 Deriving the Mathematical Model

According to **Figure 4.1** the states of a discrete-time nonlinear system are estimated using the first-order discrete-time extended Kalman filter technique. Given RK3 with states x, input u, output y, process noise w, and measurement noise v assumed as a nonlinear system.

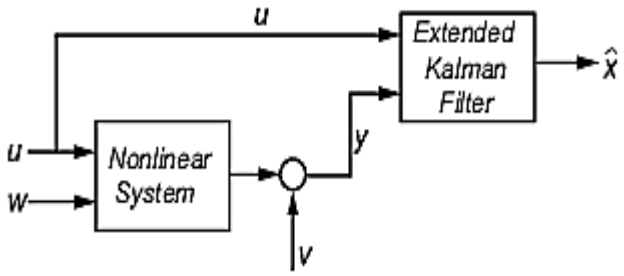

Figure 4.1: An Extended Kalman Filter block for a discrete time nonlinear system

The equation of state is thus found deciding on the state vector x in eight dimensions, x = $[T_{s1}, T_{s2}, T_{s3}, T_{s4}, T_{g1}, T_{g2}, T_{g3}, T_{g4}]^{T}$ and the control input being u = $[Q_{s,in}, Q_f, Q_{ao,} T_{s,in}, T_{a,in}]$.

The equation (4.1) is thus derived from (3.6) and (3.7), a combination of the gas and material temperatures at 8 different states as shown below;

$$
\begin{cases}
\frac{dx_1}{dt} = \frac{u_1\,(u_4 - x_1)}{ms_1 L_1} + \frac{k_{gs,1}(x_5 - x_1)}{c_{ps} m_{s,1}} - \frac{k_l\, x_1}{C_{ps} m_{s,1}} \\
\frac{dx_2}{dt} = \frac{u_1\,(x_1 - x_2)}{ms_2 L_2} + \frac{k_{gs,2}(x_6 - x_2)}{c_{ps} m_{s,2}} - \frac{k_l\, x_2}{C_{ps} m_{s,2}} \\
\frac{dx_3}{dt} = \frac{u_1\,(x_2 - x_3)}{ms_3 L_3} + \frac{k_{gs3}(x_7 - x_3)}{c_{ps} m_{s3}} - \frac{k_l\, x_3}{C_{ps} m_{s3}} \\
\frac{dx_3}{dt} = \frac{u_1\,(x_2 - x_3)}{ms_3 L_3} + \frac{k_{gs3}(x_7 - x_3)}{c_{ps} m_{s3}} - \frac{k_l\, x_3}{C_{ps} m_{s3}} \\
\frac{dx_4}{dt} = \frac{u_1\,(x_3 - x_4)}{ms_4 L_4} + \frac{k_{gs,4}(x_8 - x_4)}{c_{ps} m_{s,4}} - \frac{k_l\, x_4}{C_{ps} m_{s,4}} \\
\frac{dx_5}{dt} = \frac{\rho_{go} u_3\,(x_6 - x_5)}{m_g L_1} + \frac{k_{gs,1}(x_5 - x_1)}{c_{pg} m_g} \\
\frac{dx_6}{dt} = \frac{\rho_{go} u_3\,(x_7 - x_6)}{m_g L_2} + \frac{k_{gs,2}(x_6 - x_2)}{c_{pg} m_g} \\
\frac{dx_7}{dt} = \frac{u_3\,(\rho_{ao} x_3 - \rho_{go} x_7)}{m_g L_3} - \frac{k_{gs,3}(x_7 - x_3)}{c_{pg} m_g} - \frac{u_2 \Delta H_f}{C_{pg} m_g L_3} \\
\frac{dx_8}{dt} = \frac{\rho_{go} u_3\,(x_5 - x_8)}{m_g L_4} + \frac{k_{gs,4}(x_8 - x_4)}{c_{pg} m_g}
\end{cases}
\tag{4.1}
$$

The generated model precisely captures the heat transmission from the kiln to the bearings, considering both conductive and convective heat transfer modes. EKF conducts preliminary investigations to estimate the state of the kiln system, in which x(t) is the state to be estimated and y/z(t) the measured value, both represented by (3.12)

This equation is expressed as;

$$\dot{\boldsymbol{x}} = \boldsymbol{f}(\boldsymbol{x}, \boldsymbol{u}, \boldsymbol{t}) \tag{4.2}$$

Given the system noise being **w** as in **Figure 4.1**, the equation of state for RK3 is expressed as;

$$\dot{\boldsymbol{x}} = \boldsymbol{f}(\boldsymbol{x}, \boldsymbol{u}, \boldsymbol{t}) + \boldsymbol{w} \tag{4.3}$$

Where system noise w = $[w_1, w_2, w_3, w_4, w_5, w_6, w_7, w_8]^T$, w denotes the process noise, which accounts for disruptions in the heat transfer process dynamics.

4.1.2. Determination of Kiln Parameters

The rotary kiln used in this setup is RK3. The kiln length of 50 meters, with its respective section lengths is determined by meter markings along the kiln. The tube is found to be 3.2-meters of diameter. The stable rotation speed ranges from 1.5 to 4.2 revolutions per

minute. During operation, the shell's exterior temperature can exceed 450◦C. Temperature readings in the Celicius scale are taken for each of the four bearings at the different kiln roller stations by using a Fluke Hand Pyrometer in time intervals of 30 minutes. At the same time interval, control room display readings are taken as well for comparison purposes with ground truth (HPR). Below are 8 times steps of sample temperature readings, tabulated and analyzed using Ms Excel.

4.1.3. Determination of Algorithm Design Parameters

SPSS is used to generate a measurement noise covariance matrix **R**, representing the variance and covariance of temperature measurement noise, from a dataset of temperature readings from kiln roller bearing sensors. The resulting matrix is then used to model the uncertainty in the measurement process for the Kalman filter. Initial of 0.5 process noise **Q** = diag $[\boldsymbol{\sigma^2}_{w_1}, \boldsymbol{\sigma^2}_{w_2}, \boldsymbol{\sigma^2}_{w_3}, \boldsymbol{\sigma^2}_{w_4}, \boldsymbol{\sigma^2}_{w_5}, \boldsymbol{\sigma^2}_{w_6}, \boldsymbol{\sigma^2}_{w_7}, \boldsymbol{\sigma^2}_{w_8}]$ is obtained by assuming independent noise characteristics for each temperature variable. These are typically determined based on the characteristics of the process and measurement noise.

$$\begin{cases} \boldsymbol{w(t)} \sim (\mathbf{0}, \boldsymbol{Q}) \\ \boldsymbol{v_k} \sim (\mathbf{0}, \boldsymbol{R_k}) \end{cases} \tag{4.4}$$

Where w (t) is continuous time white noise with covariance Q, and measurement noise v_k is white noise with discrete time of covariance R_k.

The coefficients of Matrix F are symbolically obtained from the linear terms in the differential equations. Each row in Matrix F corresponds to each of the differential equations addressing the rate of change in a state variable. Other values used for calculating the state transition and control input matrices as summarized in

Table 4.1: Parameters for Filter Design. (Heat and Mass balance tool, Holcim Group Ltd, (September, 2010), (Dqg et al., 2020)

L_1	18	m_g	0.253t/h	k_{gs1}	22.67MJ/(m.K.h)
L_2	16	ΔH_f	3.276MJ/kg	k_{gs2}	21.97MJ/(m.K.h)
L_3	9.4	Amb temp	29◦C	k_{gs3}	13.85MJ/(m.K.h)
L_4	6.4	Q_f	2.5	k_{gs4}	23MJ/(m.K.h)
u_s	274.2m/h	m_s	16.67 kg/s	k_l	0.86MJ/(m.K.h)
c_{ps}	0.863KJ/Nm^3	cpg	1.3KJ/Nm3	$\boldsymbol{\rho}_{ao}$	1.293kg/Nm^3
				$\boldsymbol{\rho}_{go}$	0.905kg/Nm^3
$\boldsymbol{T_{s1}}$	950	T_{s4}	1240	T_{g3}	1450
$\boldsymbol{T_{s2}}$	1100	T_{g1}	950	T_{g4}	1240
$\boldsymbol{T_{s3}}$	1450	T_{g2}	1100		

Prediction Step

For example, x (t) is the state vector representing the process at time t, and y (t) is a known (observable) relevant vector. We suppose that the change of the process x from time t-1 to t is supplied by the system matrices and vectors listed below;

$$\text{State vector (x)} = \Delta x\,(t) = \begin{bmatrix} T_{s1} \\ T_{s2} \\ T_{s3} \\ T_{s4} \\ T_{g1} \\ T_{g2} \\ T_{g3} \\ T_{g4} \end{bmatrix} = \begin{bmatrix} 950 \\ 1100 \\ 1450 \\ 1240 \\ 950 \\ 1100 \\ 1450 \\ 1240 \end{bmatrix} \tag{4.5}$$

For simplicity, we assume that the bearing temperatures and kiln section temperatures follow a linear relationship. For the j^{th} bearing at the i^{th} zone, the bearing temperature T_b, i, j is represented as follows:

$$\text{Sensor measurements } \mathbf{y}_{(t)} = \begin{bmatrix} T_{b1,1} \\ T_{b1,2} \\ T_{b1,3} \\ T_{b1,4} \\ T_{b2,1} \\ T_{b2,2} \\ T_{b2,3} \\ T_{b2,4} \\ T_{b3,1} \\ T_{b3,2} \\ T_{b3,3} \\ T_{b3,4} \end{bmatrix} \tag{4.6}$$

According to the actual steady state condition, the input variable is given below and the parameters for the state equation presented in **Table 4.1**.

$$\Delta u\,(t) = \begin{bmatrix} Q_{s,in} \\ Q_f \\ Q_{ao} \\ T_{s,in} \\ T_{a,in} \end{bmatrix} = \begin{bmatrix} 250 \\ 2.5 \\ 109350 \\ 900 \\ 1300 \end{bmatrix} \tag{4.7}$$

If we assume independent noise for each temperature variable, matrix Q is given as;

$$\mathbf{Q} = \begin{bmatrix} \sigma^2_{w_1} & 0 & 0 & 0 & 0 & 0 & 0 & 0 \\ 0 & \sigma^2_{w_2} & 0 & 0 & 0 & 0 & 0 & 0 \\ 0 & 0 & \sigma^2_{w_3} & 0 & 0 & 0 & 0 & 0 \\ 0 & 0 & 0 & \sigma^2_{w_4} & 0 & 0 & 0 & 0 \\ 0 & 0 & 0 & 0 & \sigma^2_{w_5} & 0 & 0 & 0 \\ 0 & 0 & 0 & 0 & 0 & \sigma^2_{w_6} & 0 & 0 \\ 0 & 0 & 0 & 0 & 0 & 0 & \sigma^2_{w_7} & 0 \\ 0 & 0 & 0 & 0 & 0 & 0 & 0 & \sigma^2_{w_8} \end{bmatrix}$$

$$\mathbf{Q} = \begin{bmatrix} 0.5 & 0 & 0 & 0 & 0 & 0 & 0 & 0 \\ 0 & 0.5 & 0 & 0 & 0 & 0 & 0 & 0 \\ 0 & 0 & 0.5 & 0 & 0 & 0 & 0 & 0 \\ 0 & 0 & 0 & 0.5 & 0 & 0 & 0 & 0 \\ 0 & 0 & 0 & 0 & 0.5 & 0 & 0 & 0 \\ 0 & 0 & 0 & 0 & 0 & 0.5 & 0 & 0 \\ 0 & 0 & 0 & 0 & 0 & 0 & 0.5 & 0 \\ 0 & 0 & 0 & 0 & 0 & 0 & 0 & 0.5 \end{bmatrix} \tag{4.8}$$

R matrix (4.9)

$$\begin{bmatrix}
4.303 & -1.843 & 3.229 & -1.633 & 6.389 & -6.100 & 5.993 & -6.331 & 6.467 & -9.740 & 6.428 & -7.151 \\
-1.843 & 7.041 & 1.844 & 9.842 & -4.124 & 4.345 & -5.111 & 11.777 & -4.089 & -48.016 & -15.412 & 1.791 \\
3.229 & 1.844 & 4.465 & 3.905 & 4.149 & -4.258 & 3.085 & -0.062 & 4.636 & -39.407 & -2.472 & -6.544 \\
-1.633 & 9.842 & 3.908 & 15.087 & -4.385 & 3.700 & -6.145 & 16.360 & -3.543 & -84.374 & -22.643 & -0.182 \\
6.389 & -4.124 & 4.149 & -4.385 & 10.515 & -9.880 & 9.868 & -12.160 & 10.648 & -3.470 & 12.453 & -10.608 \\
-6.100 & 4.345 & -4.258 & 3.700 & -9.880 & 13.627 & -8.049 & 10.523 & -9.884 & 16.659 & -9.928 & 12.035 \\
5.993 & -5.111 & 3.085 & -6.145 & 9.868 & -8.049 & 11.950 & -13.373 & 10.764 & 13.277 & 15.290 & -8.364 \\
-6.331 & 11.777 & -0.062 & 16.360 & -12.160 & 10.523 & -13.373 & 28.181 & -14.834 & -67.916 & -28.347 & 8.811 \\
6.467 & -4.089 & 4.636 & -3.543 & 10.648 & -9.884 & 10.764 & -14.834 & 15.651 & -13.804 & 11.594 & -11.231 \\
-9.740 & -48.016 & -39.407 & -84.374 & -3.470 & 16.659 & 13.277 & -67.916 & -13.804 & 631.039 & 115.983 & 47.189 \\
6.428 & -15.412 & -2.472 & -22.643 & 12.463 & -9.928 & 15.290 & -28.347 & 11.594 & 115.983 & 39.640 & -4.914 \\
-7.151 & 1.791 & -6.544 & -0.182 & -10.608 & 12.035 & -8.364 & 8.811 & -11.231 & 47.189 & -4.914 & 15.624
\end{bmatrix}$$

State Transition Jacobian (A/F): The resulting discrete non-linear system equations in (4.1) are used in the EKF for calculating the a-priori estimate of the states $\hat{x}^{-}_{(k+1)}$ in the prediction step, using the a posterior estimates of the last iteration $\hat{x}^{+}_{(k)}$ from which the discrete Jacobians can be calculated as shown in (4.10). The initial values $\hat{x}^{+}_{(0)}$ are then defined.

$$\begin{bmatrix}
A_{11} & A_{21} & A_{31} & A_{41} & A_{51} & A_{61} & A_{71} & A_{81} \\
A_{12} & A_{22} & A_{32} & A_{42} & A_{52} & A_{62} & A_{72} & A_{82} \\
A_{13} & A_{23} & A_{33} & A_{43} & A_{53} & A_{63} & A_{73} & A_{83} \\
A_{14} & A_{24} & A_{34} & A_{44} & A_{54} & A_{64} & A_{74} & A_{84} \\
A_{15} & A_{25} & A_{35} & A_{45} & A_{55} & A_{65} & A_{75} & A_{85} \\
A_{16} & A_{26} & A_{36} & A_{46} & A_{56} & A_{66} & A_{76} & A_{86} \\
A_{17} & A_{27} & A_{37} & A_{47} & A_{57} & A_{67} & A_{77} & A_{87} \\
A_{18} & A_{28} & A_{38} & A_{48} & A_{58} & A_{68} & A_{78} & A_{88}
\end{bmatrix} \tag{4.10}$$

The discrete Jacobian can be calculated symbolically in this matrix as,

$$\mathbf{A_{11}} = -\frac{u_1}{m_{s1}L_1} - \frac{k_{gs,1}}{c_{ps}m_{s1}} - \frac{k_l}{c_{ps}m_{s1}} \tag{4.11}$$

$$\mathbf{A_{22}} = -\frac{u_1}{m_{s2}L_2} - \frac{k_{gs,2}}{c_{ps}m_{s2}} - \frac{k_l}{c_{ps}m_{s2}} \tag{4.12}$$

$$\mathbf{A_{12}} = \frac{u_1}{m_2 L_2} \qquad \mathbf{A_{23}} = \frac{u_1}{m_{s3}L_3} \qquad \mathbf{A_{15}} = \frac{\rho_{g0}u_3}{m_g L_1} \tag{4.13}$$

$$\mathbf{A_{26}} = \frac{\rho_{g0}u_3}{m_g L_2} \qquad \mathbf{A_{33}} = -\frac{u_1}{m_{s3}L_3} - \frac{k_{gs,3}}{c_{ps}m_3} - \frac{k_l}{c_{ps}m_{s3}} \tag{4.14}$$

$$\mathbf{A_{34}} = \frac{u_1}{m_{s4}L_4} \quad \mathbf{A_{37}} = \frac{\rho_{a0}u_3}{m_g L_3} \quad \mathbf{A_{44}} = -\frac{u_1}{m_4 L_4} - \frac{k_{g,s4}}{c_{ps}m_{s4}} \frac{k_l}{c_{ps}m_{s4}} \tag{4.15}$$

$$\mathbf{A_{48}} = \frac{\rho_{go}u_3}{m_g L_4} \qquad \mathbf{A_{51}} = \frac{k_{gs,1}}{c_{ps}m_{s1}} \qquad \mathbf{A_{55}} = -\frac{\rho_{go}u_3}{m_g L_1} - \frac{k_{gs,1}}{c_{pg}m_g} \tag{4.16}$$

$$\mathbf{A_{62}} = \frac{k_{gs,2}}{c_{ps}m_{s2}} \quad \mathbf{A_{66}} = -\frac{\rho_{go}u_3}{m_g L_2} - \frac{k_{gs,2}}{c_{pg}m_g} \tag{4.17}$$

$$\begin{bmatrix} 0.6036 & 0 & 0 & 0 & 153.255 & 0 & 0 & 0 \\ 1.028 & 2.6145 & 0 & 0 & 0 & 0.6391 & 0 & 0 \\ 0 & 1.7499 & 18.0141 & 0 & 0 & 0 & 1.0461 & 0 \\ 0 & 0 & 2.5701 & 1.9151 & 0 & 0 & 0 & 1.0461 \\ 54.491 & 0 & 0 & 0 & 57.546 & 0 & 0 & 0 \\ 0 & 61.302 & 0 & 0 & 0 & 167.78 & 0 & 0 \\ 0 & 0 & 104.34 & 0 & 0 & 0 & 167.8 & 290.5 \\ 0 & 0 & 0 & 153.255 & 0 & 0 & 0 & 223.185 \end{bmatrix} \quad (4.18)$$

The representation of the influence of control inputs on the state variables and applies to the control vector u_t at time t,

$$\begin{bmatrix} \frac{u_4}{m_{s1}L_1} & 0 & 0 & \frac{-1}{m_{s1}L_1} & 0 \\ \frac{u_1}{m_{s2}L_2} & 0 & 0 & 0 & 0 \\ \frac{u_1}{m_{s3}L_3} & 0 & 0 & 0 & 0 \\ \frac{u_1}{m_{s4}L_4} & 0 & 0 & 0 & 0 \\ 0 & 0 & \frac{\rho_{go}}{m_g L_1} & 0 & 0 \\ 0 & 0 & \frac{\rho_{go}}{m_g L_2} & 0 & 0 \\ 0 & -\frac{\Delta H_f}{c_{pg} m_g L_3} & \frac{\rho_{ao}}{m_g L_3} & 0 & 0 \\ 0 & 0 & \frac{\rho_{go}}{m_g L_4} & 0 & 0 \end{bmatrix}$$

$$\begin{bmatrix} 0.914 & 0 & 0 & 0.003 & 0 \\ 0.914 & 0 & 0 & 0 & 0 \\ 0.914 & 0 & 0 & 0 & 0 \\ 0.914 & 0 & 0 & 0 & 0 \\ 0 & 0 & 0.198 & 0 & 0 \\ 0 & 0 & 0.223 & 0 & 0 \\ 0 & 1.059 & 0.543 & 0 & 0 \\ 0 & 0 & 1.465 & 0 & 0 \end{bmatrix} \quad (4.19)$$

Covariance prediction: The a-priori covariance estimate can be defined as;

$$\mathbf{P}^{-}_{(k+1)} = \mathbf{F}_{(k+1)}\, \mathbf{P}^{+}_{(k)}\, \mathbf{F}_{(k+1)}{}^{T} + \mathbf{Q}. \quad (4.20)$$

In the initially calculated time step, P+ (0) is expressed by initial estimates; otherwise, it represents the preceding time step's a posteriori estimate. The process noise (4.8) is added to account for the model inaccuracies.

With a standard deviation of 0.03 for all state variables, the variances were initialized as 0.0009 as shown in (4.21);

$$\begin{bmatrix} \sigma^2{}_{x_1} & 0 & 0 & 0 & 0 & 0 & 0 & 0 \\ 0 & \sigma^2{}_{x_2} & 0 & 0 & 0 & 0 & 0 & 0 \\ 0 & 0 & \sigma^2{}_{x_3} & 0 & 0 & 0 & 0 & 0 \\ 0 & 0 & 0 & \sigma^2{}_{x_4} & 0 & 0 & 0 & 0 \\ 0 & 0 & 0 & 0 & \sigma^2{}_{x_5} & 0 & 0 & 0 \\ 0 & 0 & 0 & 0 & 0 & \sigma^2{}_{x_6} & 0 & 0 \\ 0 & 0 & 0 & 0 & 0 & 0 & \sigma^2{}_{x_7} & 0 \\ 0 & 0 & 0 & 0 & 0 & 0 & 0 & \sigma^2{}_{x_8} \end{bmatrix}$$

$\boldsymbol{P^+}$ **(0)** =

$$\begin{bmatrix} 0.0009 & 0 & 0 & 0 & 0 & 0 & 0 & 0 \\ 0 & 0.0009 & 0 & 0 & 0 & 0 & 0 & 0 \\ 0 & 0 & 0.0009 & 0 & 0 & 0 & 0 & 0 \\ 0 & 0 & 0 & 0.0009 & 0 & 0 & 0 & 0 \\ 0 & 0 & 0 & 0 & 0.0009 & 0 & 0 & 0 \\ 0 & 0 & 0 & 0 & 0 & 0.0009 & 0 & 0 \\ 0 & 0 & 0 & 0 & 0 & 0 & 0.0009 & 0 \\ 0 & 0 & 0 & 0 & 0 & 0 & 0 & 0.0009 \end{bmatrix} \quad (4.21)$$

Measurement Update

Here the EKF based method refines the state estimate by incorporating new measurements. The Kalman gain is calculated to evaluate how much to trust the measurements in comparison to the prediction;

$$\mathbf{K_{(k+1)} = P^-_{(k+1)} H^T (HP^-_{(k+1)} H^T + R)^{-1}} \quad (4.22)$$

As previously discussed in (4.10), the best way to linearize an equation at a point is to find its jacobian, which we do by taking its derivative in (4.14).

$$\mathrm{H} = \frac{\partial h}{\partial x} = \begin{bmatrix} \frac{\partial h_1}{\partial x_1} & \cdots & \frac{\partial h_1}{\partial x_8} \\ \vdots & \ddots & \vdots \\ \frac{\partial h_8}{\partial x_1} & \cdots & \frac{\partial h_8}{\partial x_8} \end{bmatrix}$$

$$\begin{bmatrix} 0.7 & 0 & 0 & 0 & 0.3 & 0 & 0 & 0 \\ 0.7 & 0 & 0 & 0 & 0.3 & 0 & 0 & 0 \\ 0 & 0.7 & 0 & 0 & 0 & 0.3 & 0 & 0 \\ 0 & 0.7 & 0 & 0 & 0 & 0.3 & 0 & 0 \\ 0 & 0 & 0.7 & 0 & 0 & 0 & 0.3 & 0 \\ 0 & 0 & 0.7 & 0 & 0 & 0 & 0.3 & 0 \\ 0 & 0 & 0 & 0.7 & 0 & 0 & 0 & 0.3 \\ 0 & 0 & 0 & 0.7 & 0 & 0 & 0 & 0.3 \\ 0.7 & 0 & 0 & 0 & 0.3 & 0 & 0 & 0 \\ 0.7 & 0 & 0 & 0 & 0.3 & 0 & 0 & 0 \\ 0 & 0.7 & 0 & 0 & 0 & 0.3 & 0 & 0 \\ 0 & 0.7 & 0 & 0 & 0 & 0.3 & 0 & 0 \end{bmatrix} \quad (4.23)$$

The anticipated state is updated with the measurement, weighted by the Kalman gain, as shown in (4.24).

$$\hat{\boldsymbol{x}}_{\boldsymbol{k}} = \hat{\boldsymbol{x}}_{\boldsymbol{k}}^{-} + \boldsymbol{K}_{\boldsymbol{k}} \left(\boldsymbol{z}_{\boldsymbol{k}} - \mathbf{h}(\hat{\boldsymbol{x}}_{\boldsymbol{k}}^{-})\right) \quad (4.24)$$

Where $z_k - h(\hat{x}_k^-)$ is the measurement residual.

Following the measurement update (4.16), the error covariance is modified to reflect the reduced uncertainty, as seen below;

$$\mathbf{P_k} = (\mathbf{I} - \mathbf{K_k}\,\mathbf{H_k})\,\mathbf{P_k^-} \quad (4.25)$$

The block generates state estimates for the current time step by combining the system's state transition and measurement functions with the Extended Kalman Filter method. The above prediction and update steps are repeated for each time step k, progressively refining the state estimate and its uncertainty.

4.2 Simplified Extended Kalman Filter Model

Due to the complexity and computational demands of more detailed models, a simplified Kalman filter is implemented. This choice is motivated by;

i. The need for a practical and timely solution

ii. Facilitating model understanding and ease of use in the control room environment.

iii. The ability to deliver consistent and reliable temperature estimates in the short term.

4.2.1 Filter Equations

To integrate the model into a Kalman Filter, the system is represented in a state-space form:

$$\begin{cases} \boldsymbol{x_{k+1}} = \boldsymbol{A_{x_k}} + \boldsymbol{Bu_k} + \boldsymbol{w_k} \\ \boldsymbol{y_k} = \boldsymbol{H_{x_k}} + \boldsymbol{v_k} \end{cases} \tag{4.26}$$

Such that; x_k is the vector of state variable, kiln zone temperatures, u_k represents control inputs, w_k is process noise and v_k is the measurement noise (uncertainty or error in the bearing temperature measurements), y_k is the vector of measured values being bearing temperatures and H is the measurement matrix that relates the system state to the measurements, and in this example, the bearing temperatures.

4.2.2 Filter Implementation

Initialization

The filter in (4.26) is initialized with a state vector of size 8, representing different temperature metrics, a state transition matrix A, control input matrix B for modeling dynamics and inputs. A noise covariance matrices Q and R for process and measurement uncertainties and an error covariance matrix P initialized with high values to signify initial uncertainty.

State Transition

Depicts how the kiln's temperature changes over time. Due to slow heat transmission mechanisms in the kiln's material and gas, 95% of the system's former state is retained. Because heat from one section of the kiln adds slightly to the next, the 0.05% at the sub-diagonal represents the coupling between neighboring states due to heat transfer.

$$A = \begin{bmatrix} 0.95 & 0 & 0 & 0 & 0.05 & 0 & 0 & 0 \\ 0.05 & 0.95 & 0 & 0 & 0 & 0.05 & 0 & 0 \\ 0 & 0.05 & 0.95 & 0 & 0 & 0 & 0.05 & 0 \\ 0 & 0 & 0.05 & 0.95 & 0 & 0 & 0 & 0.05 \\ 0.05 & 0 & 0 & 0 & 0.95 & 0 & 0 & 0 \\ 0 & 0.05 & 0 & 0 & 0 & 0.95 & 0 & 0 \\ 0 & 0 & 0.05 & 0 & 0 & 0 & 0.95 & 0 \\ 0 & 0 & 0 & 0.05 & 0 & 0 & 0 & 0.95 \end{bmatrix} \quad (4.27)$$

Control Matrix

Material temperature is influenced more significantly (0.5) than gas temperature (0.3) because the material is denser and keeps heat longer. The gas phase is more active and releases heat more quickly due to convection and flow, even though it absorbs energy from the same sources.

$$\mathbf{B} = \begin{bmatrix} 0.5 & 0 & 0 & 0 & 0 \\ 0.5 & 0 & 0 & 0 & 0 \\ 0.5 & 0 & 0 & 0 & 0 \\ 0.5 & 0 & 0 & 0 & 0 \\ 0 & 0.3 & 0.3 & 0.3 & 0.3 \\ 0 & 0.3 & 0.3 & 0.3 & 0.3 \\ 0 & 0.3 & 0.3 & 0.3 & 0.3 \\ 0 & 0.3 & 0.3 & 0.3 & 0.3 \end{bmatrix} \quad (4.28)$$

Process Noise Covariance Matrix (Q)

Because of the degree of uncertainty in the state transition process such as the dynamics that weren't modeled, the process noise is relatively small compared to the state values thus ensuring that the Kalman filter does not overly rely on the model when there are deviations. Otherwise it can be adjusted through calibration to improve the filter's performance.

$$\mathbf{Q} = \begin{bmatrix} 0.5 & 0 & 0 & 0 & 0 & 0 & 0 & 0 \\ 0 & 0.5 & 0 & 0 & 0 & 0 & 0 & 0 \\ 0 & 0 & 0.5 & 0 & 0 & 0 & 0 & 0 \\ 0 & 0 & 0 & 0.5 & 0 & 0 & 0 & 0 \\ 0 & 0 & 0 & 0 & 0.5 & 0 & 0 & 0 \\ 0 & 0 & 0 & 0 & 0 & 0.5 & 0 & 0 \\ 0 & 0 & 0 & 0 & 0 & 0 & 0.5 & 0 \\ 0 & 0 & 0 & 0 & 0 & 0 & 0 & 0.5 \end{bmatrix} \quad (4.29)$$

Measurement Matrix (H):

The state vector (x) is mapped to the measurement vector (H), with H assumed to be an identity matrix. This assumes that the temperature sensors provide direct measurements of the kiln's status variables.

$$\mathrm{H} = \begin{bmatrix} 1 & 0 & 0 & 0 & 0 & 0 & 0 & 0 \\ 0 & 1 & 0 & 0 & 0 & 0 & 0 & 0 \\ 0 & 0 & 1 & 0 & 0 & 0 & 0 & 0 \\ 0 & 0 & 0 & 1 & 0 & 0 & 0 & 0 \\ 0 & 0 & 0 & 0 & 1 & 0 & 0 & 0 \\ 0 & 0 & 0 & 0 & 0 & 1 & 0 & 0 \\ 0 & 0 & 0 & 0 & 0 & 0 & 1 & 0 \\ 0 & 0 & 0 & 0 & 0 & 0 & 0 & 1 \end{bmatrix} \quad (4.30)$$

Measurement Noise Covariance Matrix (R):

This matrix is used to display the measuring noise, including erratic variations or inaccurate sensor readings. Since high-precision temperature sensors typically have errors on the order of a fraction of a degree.0.1 is used for simplicity

$$\mathbf{R} = \begin{bmatrix} 0.1 & 0 & 0 & 0 & 0 & 0 & 0 & 0 \\ 0 & 0.1 & 0 & 0 & 0 & 0 & 0 & 0 \\ 0 & 0 & 0.1 & 0 & 0 & 0 & 0 & 0 \\ 0 & 0 & 0 & 0.1 & 0 & 0 & 0 & 0 \\ 0 & 0 & 0 & 0 & 0.1 & 0 & 0 & 0 \\ 0 & 0 & 0 & 0 & 0 & 0.1 & 0 & 0 \\ 0 & 0 & 0 & 0 & 0 & 0 & 0.1 & 0 \\ 0 & 0 & 0 & 0 & 0 & 0 & 0 & 0.1 \end{bmatrix} \quad (4.31)$$

The state covariance matrix, or **P matrix,** represents the degree of uncertainty in the state estimations and is amended at each step**.** The assumption here is that the errors in each of these 8 states are unrelated with a variance of 0.1 for diagonal elements

P = diag. (0.1, 0.1, 0.1, 0.1, 0.1, 0.1, 0.1, 0.1)

4.2.3. Implementation of the Python Code

An Advanced Kalman Filter is used in the code to examine temperature data from the twelve rotary kiln bearings. It consists of a state transition matrix, a control input matrix, a measurement matrix, and noise covariance matrices.

The system state is estimated using system dynamics and control inputs such as Kiln speed (2.1 - 4.2 rpm), Volume loading (8 - 12 %), Air/oxygen ratio (0.8), Ambient inlet (23◦C - 27◦C), Ambient air temperature (23◦C- 27◦C).

Kalman Gain is used to correct the system state in response to new measurements. Graphs are plotted to display the original temperature data, anticipated states before correction and corrected states (Kalman-filtered temperatures).

4.3 Experimental Verification

4.3.1 Temperature Measurements

Temperature sensors, HPR and thermocouples with known accuracy, precision, and response time are used to collect temperature measurements under the varying kiln operating conditions. These sensors are selected based on their ability to perform reliably in the high-temperature and dynamic environment of the rotary kiln.

4.3.2 Discussion of Graphical Results

The bearing temperature graphs show both raw and processed data, indicating irregularities. **Figure 4.1** shows system inputs $\boldsymbol{u}$, measurement noise $\boldsymbol{v}$, process noise $\boldsymbol{w}$, and sensor measurements $\boldsymbol{y}$. The Extended Kalman Filter uses sensor readings to provide corrected state estimations $\hat{\boldsymbol{x}}$ for the system.

4.3.2.1 Experimental Category 1

The noise attenuation capability of the KF algorithm is validated in this study by testing it with particular bearing data defining the problem statement, as demonstrated in **Figure 1 (b), (c),** and **(d)** for **(Tb1,1), (Tb1,2),** and **(Tb3,2)**. The results for all the three scenarios are plotted as **Figures 4.2, 4.3** and **4.4** respectively, where the blue solid line represents the CCR as raw sensor measurements before any filtering is done, HPR is represented by the green solid line as the ground truth data and $\hat{x}$ is the Kalman Corrected temperature represented by the red dotted line as filtered estimates accounting for measurement noise.

In all scenarios, the CCR measurements appear consistently higher than the temperature predicted values $\hat{x}$.

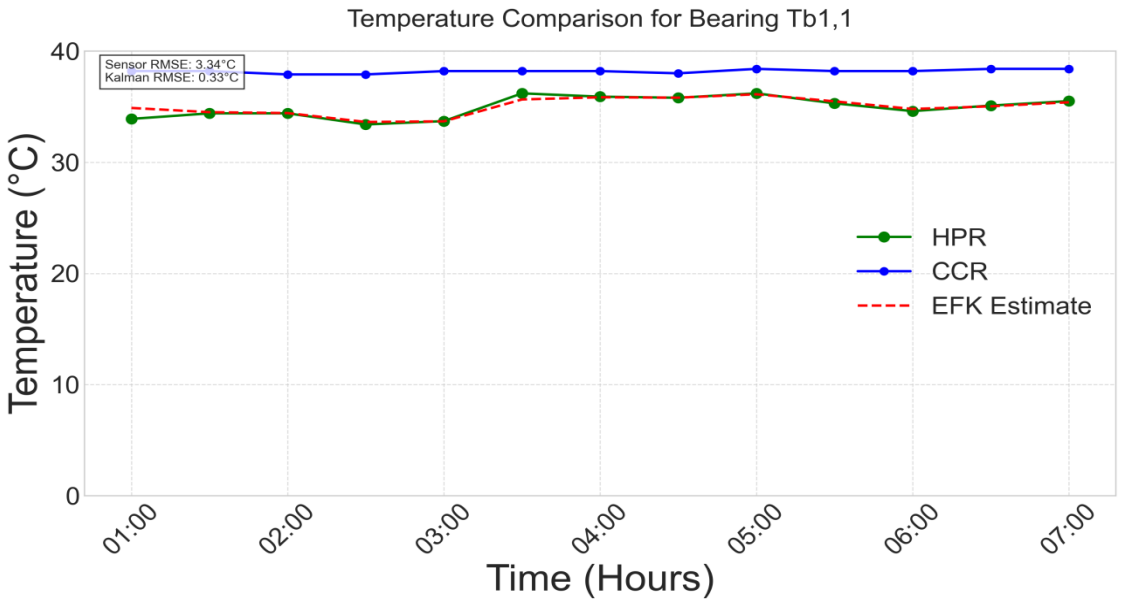

Figure 4.2: Bearing 1 temperature at tire 1

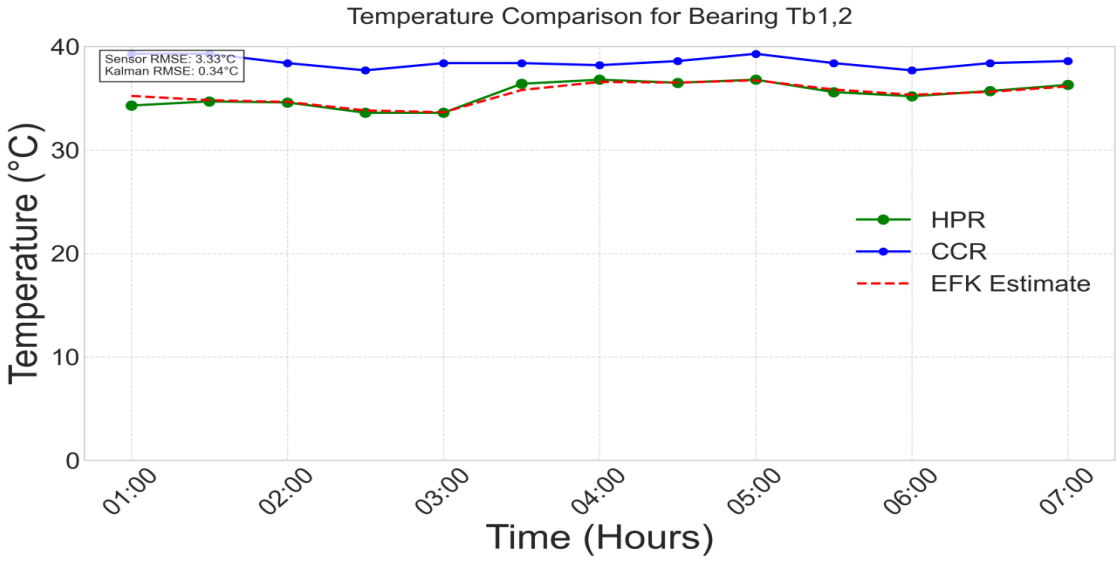

Figure 4. 3: Bearing 2 temperature at tire 1

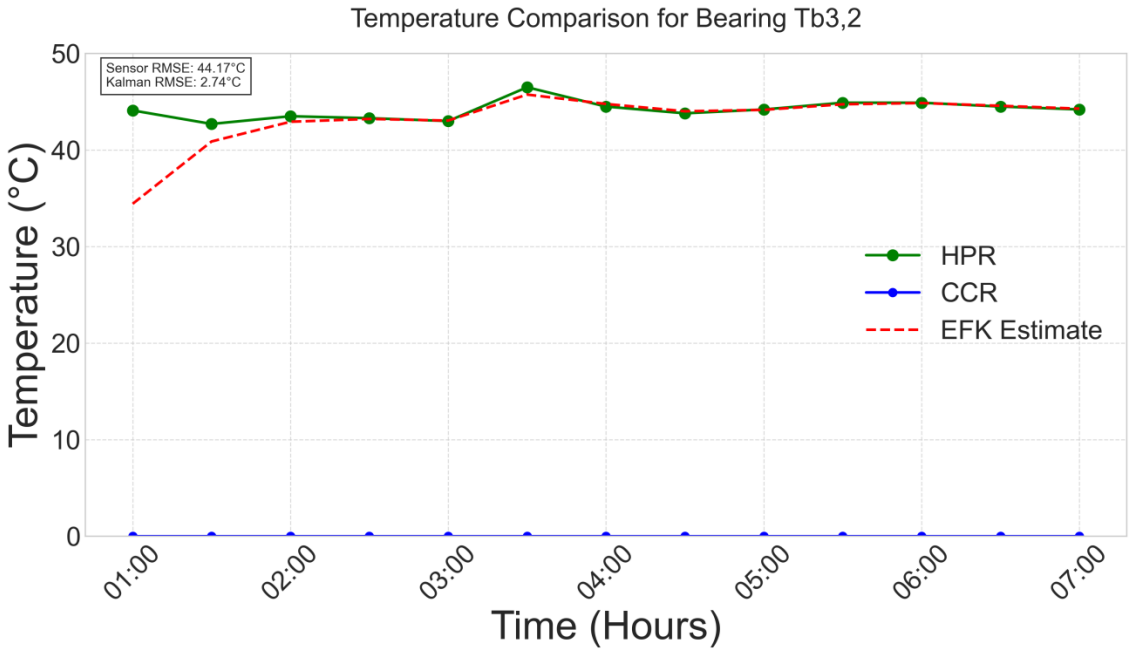

Figure 4. 4: Bearing 2 temperature at tire 3

In contrast, CCR measurements in **Figure 4.4** show a large deviation from the ground truth values. This deviation is clearly observed in the estimation error plots as well. The large difference between CCR and $\hat{x}$ could be attributed to sensor malfunctioning and external factors affecting sensor readings, such as thermal lags or local heat changes.

The EKF Algorithm thus tracks ground truth readings (HPR) demonstrating its ability to automatically detect and compensate for time- dependent discrepancies and suppress measurement errors.

From **Figure 1.3** the magnitude in error of the three bearings under consideration was suppressed as shown in **Figure 4.5** below;

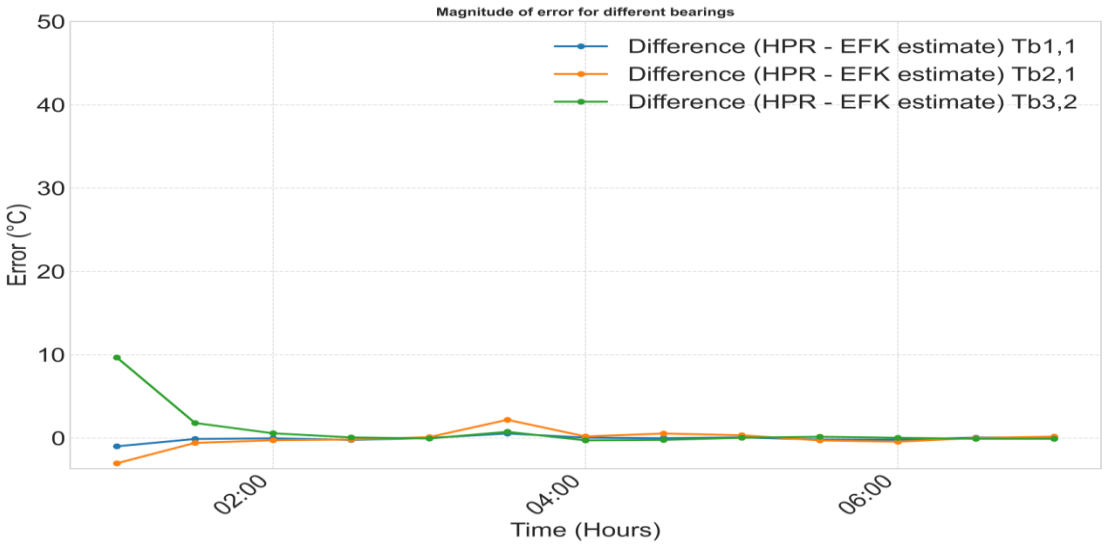

Figure 4.5: Attenuated error margin for the three selected bearings

Tables 4.2 and 4.3 below represent the temperature measurements obtained by hand pyrometer and records from control room respectively. These form part of the inputs into the Kalman filter framework at each time step to derive Kalman corrected estimates in the code block

Table 4.2: HPR (Ground Truth)

	0100hrs	**0130hrs**	**0200hrs**	**0230hrs**	**0300hrs**	**0330hrs**	**0400hrs**	**0430hrs**
Tb1,1	33.9	34.4	34.4	33.4	33.7	36.2	35.9	35.8
Tb1,2	34.3	34.7	34.6	33.6	33.6	36.4	36.8	36.5
Tb1,3	34	34.9	36.5	32.6	34.9	38	37.4	37.5
Tb1,4	34.5	35.1	36.5	34.8	34.3	37.9	37.2	37.2
Tb2,1	39.5	39.9	39.3	38.8	39.5	49.4	48.1	50.4
Tb2,2	42.2	43.6	42.8	46.3	42.5	49.6	47.8	47.5
Tb2,3	40.2	43.5	46	46.3	44.8	52.9	52.2	53
Tb2,4	40.3	41.1	44.9	47.1	42.6	57.8	56.7	56.5
Tb3,1	36	39.2	39.6	38.7	38.8	40.6	39.3	39.4
Tb3,2	44.1	42.7	43.5	43.3	43	46.5	44.5	43.8
Tb3,3	40	41.1	43.4	41.5	43.7	44.5	43.5	44.4
Tb3,4	42.5	43.5	44.6	40.9	44.8	45.7	45.2	45.5

Table 4.3: CCR readings

	0100hrs	0130hrs	0200hrs	0230hrs	0300hrs	0330hrs	0400hrs	0430hrs
Tb1, 1	38.2	38.2	37.9	37.9	38.2	38.2	38.2	38
Tb1, 2	39.3	39.3	38.4	37.7	38.4	38.4	38.2	38.6
Tb1, 3	39.3	39.3	39.3	39.3	39.4	39.5	37.9	39.5
Tb1, 4	42.7	42.5	42.7	42.7	42.7	42.7	42.7	42.7
Tb2, 1	51.8	51.8	51.8	51.8	52.2	52.2	52.4	52.9
Tb2, 2	49.9	50.2	49.7	49.9	50.2	50.4	50.2	50.4
Tb2, 3	49.5	49.7	49.9	50.2	44.8	52.2	50.9	51.3
Tb2, 4	59.3	58.7	59.8	59.2	58.8	58.3	58.8	59
Tb3, 1	49.3	49	49	49.1	49	49.3	49	49
Tb3, 2	0	0	0	0	0	0	0	0
Tb3, 3	41.1	41.1	41.3	41.6	41.6	41.6	41.6	41.6
Tb3, 4	46.3	46.3	46.3	46.4	46.5	46.5	46.6	46.8

4.3.2.2. Experimental Category 2

When testing with extra bearing data, the EKF algorithm enhances accuracy by combining model predictions with actual measurements. This leads to accurate bearing temperature monitoring, as seen in **Figures 4.4, 4.5, 4.6, 4.7,** and **4.8**.

In **Figure 4.5**, a temperature drop between 0200hrs and 0300hrs is recorded by both HPR and EKF, indicating an operational change in the system. However this drop is not captured by the sensor readings.

In **Figure 4.6**, there is a temperature rise at 0200hrs, followed by a drop 30minutes later. Another increase is again observed up to 0330hrs. These deviations are not captured by the central control room sensor based measurements as well implying that the robust and trusting the hand pyrometer readings, the standard measure herein.

Figure 4.7 depicts the temperature profile of Bearing Tb2, 4 over time. It compares CCR data to EKF-estimated values $\hat{x}$ and a reference HPR. The EKF suppresses sensor noise while monitoring temperature changes. Around 0330hrs, a temperature rise is reliably recorded, and around 0600hrs, a sudden sensor drop is filtered out, validating EKF's robustness. The EKF improves accuracy by balancing model predictions with real data, making it useful for predictive maintenance in the rotary kiln system.

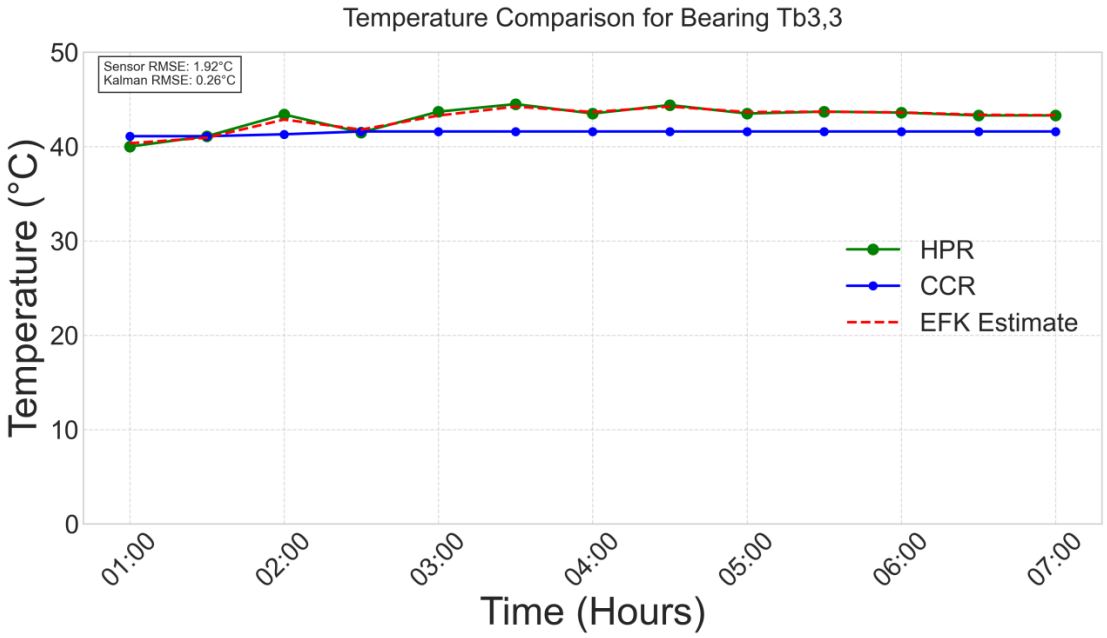

Figure 4.6: Bearing 3 temperature at tire 3

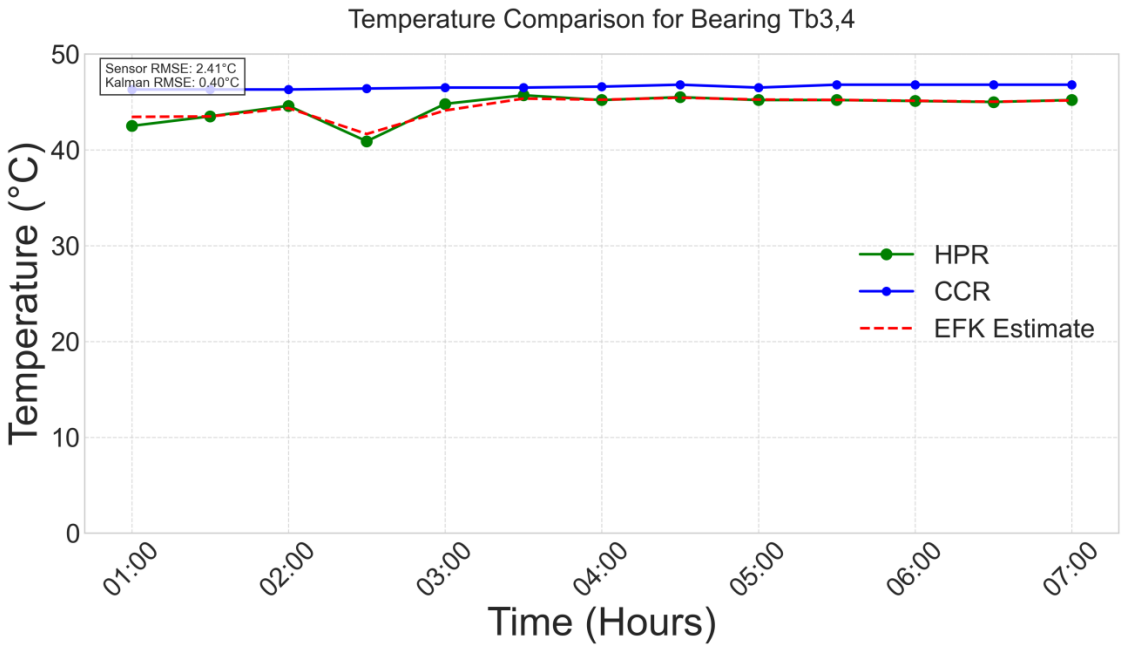

Figure 4.7:Bearing 4 temperature at tire 3

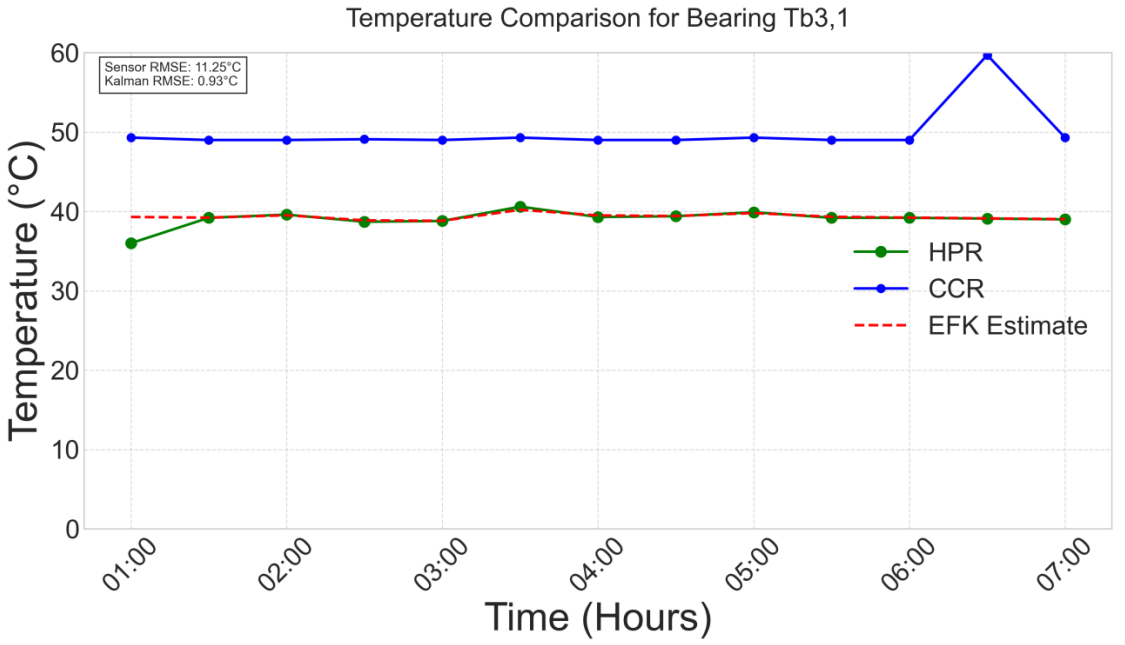

Figure 4. 8: Bearing 1 temperature at tire 3

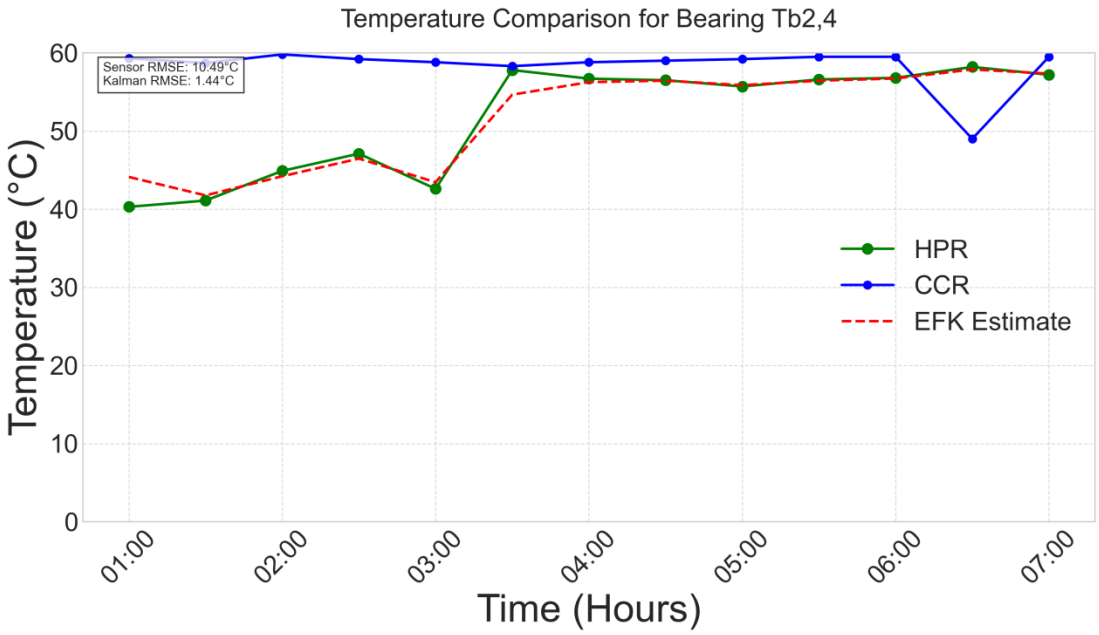

Figure 4. 9: Bearing 4 temperature at tire 2

In **Figure 4.8** and **4.9**, there was a sharp increase and decline in temperature measurements respectively between 0600hrs and 0700hrs yet the Kalman filter estimates trusted the hand pyrometer readings. In both instances, the sensor noise is filtered out proving the robustness of the algorithm. In **Figure 4.10**, the sensor readings were constant all through which was an indication of a frozen value in control room yet the algorithm managed to produce reliable estimates based on the hand pyrometer readings, proving the accuracy of the algorithm.

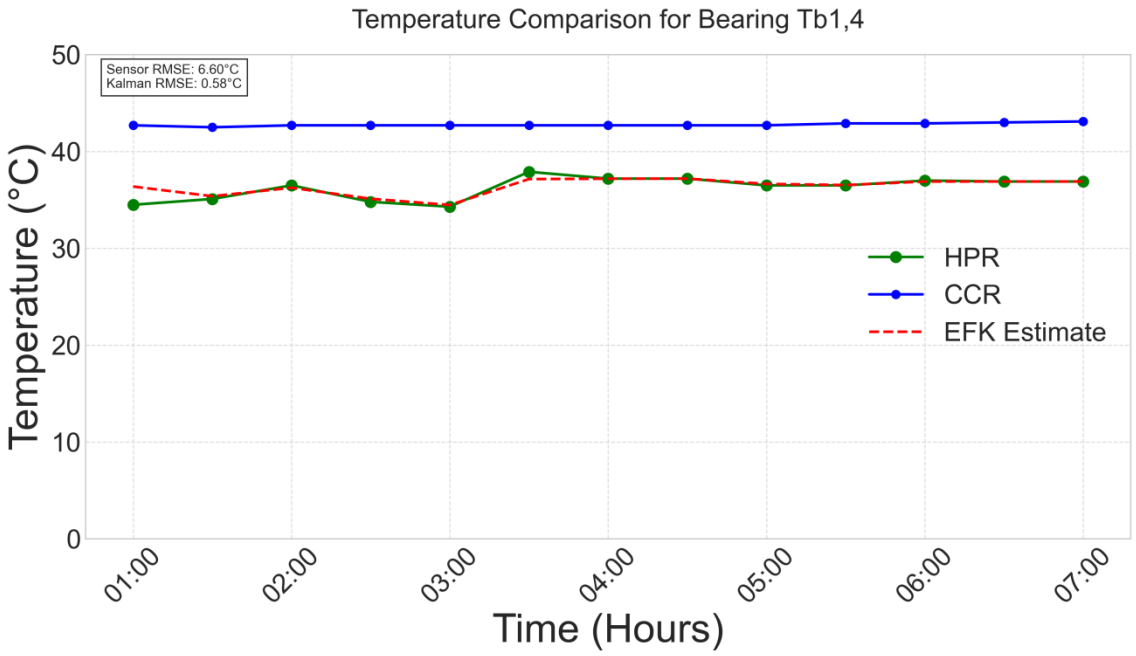

Figure 4.10: Bearing temperature 4 at tire 1

4.3.3. Establishing the RMSE and MAE

The EKF temperature estimates are compared to sensor measurement data to evaluate its filtering accuracy and noise reduction capabilities. The Root Mean Square Error (RMSE) quantifies differences between estimated and actual measurements.

Appendix C shows computation of the RMSE code block by comparing $\hat{\boldsymbol{x}}$ and CCR measurements against the HPR data for each timestamp.

The resulting RMSE values quantify the accuracy of the filter's estimates and are summarized in the **Table 4.4** which provides a clear numerical representation of the filter's performance by showing how closely the $\hat{\boldsymbol{x}}$ values and CCR data align with the actual ground truth, enabling validation of the Extended Kalman Filter's effectiveness. The filter shows the ability to smooth noisy measurements while retaining true temperature trends.

Table 4.4: Cross-validation summary for the RMSE values for the different sets of data

Bearing Tb1,1:	**Bearing Tb1,2:**	**Bearing Tb1,3:**
Sensor vs Ground Truth: RMSE: 3.343°C Kalman vs Ground Truth: RMSE: 0.207°C Kalman Filter Improvement: 93.8%	Sensor vs Ground Truth: RMSE: 3.325°C Kalman vs Ground Truth: RMSE: 0.239°C Kalman Filter Improvement: 92.8%	Sensor vs Ground Truth: RMSE: 3.416°C Kalman vs Ground Truth: RMSE: 0.421°C Kalman Filter Improvement: 87.7%
Bearing Tb1,4: Sensor vs Ground Truth: RMSE: 6.603°C Kalman vs Ground Truth: RMSE: 0.290°C Kalman Filter Improvement: 95.6%	**Bearing Tb2,1:** Sensor vs Ground Truth: RMSE: 8.260°C Kalman vs Ground Truth: RMSE: 0.892°C Kalman Filter Improvement: 89.2%	**Bearing Tb2,2:** Sensor vs Ground Truth: RMSE: 4.808°C Kalman vs Ground Truth: RMSE: 0.551°C Kalman Filter Improvement: 88.5%
Bearing Tb2,3: Sensor vs Ground Truth: RMSE: 3.876°C Kalman vs Ground Truth: RMSE: 1.062°C Kalman Filter Improvement: 72.6%	**Bearing Tb2,4:** Sensor vs Ground Truth: RMSE: 10.490°C Kalman vs Ground Truth: RMSE: 1.422°C Kalman Filter Improvement: 86.4%	**Bearing Tb3,1:** Sensor vs Ground Truth: RMSE: 11.253°C Kalman vs Ground Truth: RMSE: 0.283°C Kalman Filter Improvement: 97.5%
Bearing Tb3,2: Sensor vs Ground Truth: RMSE: 44.172°C Kalman vs Ground Truth: RMSE: 0.255°C Kalman Filter Improvement: 99.4%	**Bearing Tb3,3:** Sensor vs Ground Truth: RMSE: 1.916°C Kalman vs Ground Truth: RMSE: 0.307°C Kalman Filter Improvement: 84%	**Bearing Tb3,4:** Sensor vs Ground Truth: RMSE: 2.411°C Kalman vs Ground Truth: RMSE: 0.350°C Kalman Filter Improvement: 85.5%

Table 4.5:Cross-Validation summary for the MAE value for the different sets of data

Bearing Tb1,1:	**Bearing Tb1,2:**	**Bearing Tb1,3:**
Sensor vs Ground Truth: MAE: 3.231°C Kalman vs Ground Truth: MAE: 0.200°C Kalman Filter Improvement: 93.8%	Sensor vs Ground Truth: MAE: 3.123°C Kalman vs Ground Truth: MAE: 0.223°C Kalman Filter Improvement: 92.9%	Sensor vs Ground Truth: MAE: 2.969◦C Kalman vs Ground Truth: MAE: 0.322°C Kalman Filter Improvement: 89.2%
Bearing Tb1,4: Sensor vs Ground Truth: MAE: 6.515°C Kalman vs Ground Truth: MAE: 0.304°C Kalman Filter Improvement: 95.3%	**Bearing Tb2,1:** Sensor vs Ground Truth: MAE: 6.969°C Kalman vs Ground Truth: MAE: 0.640°C Kalman Filter Improvement: 90.8%	**Bearing Tb2,2:** Sensor vs Ground Truth: MAE: 4.131°C Kalman vs Ground Truth: MAE: 0.425°C Kalman Filter Improvement: 89.7%
Bearing Tb2,3: Sensor vs Ground Truth: MAE: 2.854°C Kalman vs Ground Truth: MAE: 0.507°C Kalman Filter Improvement: 82.2%	**Bearing Tb2,4:** Sensor vs Ground Truth: MAE: 8.115°C Kalman vs Ground Truth: MAE: 0.860°C Kalman Filter Improvement: 89.4%	**Bearing Tb3,1:** Sensor vs Ground Truth: MAE: 10.846°C Kalman vs Ground Truth: MAE: 0.349°C Kalman Filter Improvement: 96.8%
Bearing Tb3,2: Sensor vs Ground Truth: MAE: 44.162°C Kalman vs Ground Truth: MAE: 1.064°C Kalman Filter Improvement: 97.6%	**Bearing Tb3,3:** Sensor vs Ground Truth: MAE: 1.723°C Kalman vs Ground Truth: MAE: 0.203°C Kalman Filter Improvement: 88.2%	**Bearing Tb3,4:** Sensor vs Ground Truth: MAE: 2.077°C Kalman vs Ground Truth: MAE: 0.249°C Kalman Filter Improvement: 88.0%

4.3.4 Evaluation of the Kalman Filter's Overall Performance and Accuracy

From **Table 4.4**, the RMSE for various data sets are acquired, and the Extended Kalman Filter is evaluated for its potential to improve temperature measurement accuracy, as demonstrated below:

a) The overall Root Mean Square Error (RMSE) for sensor measurements is found to be **8.656°C**.

b) Kalman-corrected RMSE: Temperature readings with Kalman correction had a lower RMSE of **0.523°C.**

c) Average MAE for sensor measurements: **8.060°C**

d) Average Kalman corrected MAE: **0.445°C**

e) Error Reduction (RMSE improvement): A **94.0%** improvement in measurement accuracy.

f) MAE improvement : **94.5%**

CHAPTER FIVE: SUMMARY OF RESULTS, CONCLUSION AND RECOMMENDATIONS

This chapter consists of an overview of results, conclusions, along with suggestions for future work to be done.

5.1. Summary of results

Implementing the Extended Kalman Filter (EKF) on kiln temperature data decreased the average Root Mean Square Error (RMSE) from 8.656 °C (raw sensor values) to 0.523 °C, signifying a 94% enhancement in measurement precision. The nearly similar percentage improvement in RMSE and MAE implies that the correction is not only decreasing average error, but also suppressing variations in residual errors after filtering. This significant reduction suggests that the filter efficiently reduces the impact of sensor noise and process irregularities. Similar improvements were documented in comparable thermal process experiments. For instance, in his design of a good state estimator for a furnace at a thermal power plant, Nair, 2011 used the Linear Kalman Filter and Extended Kalman Filter algorithms, and simulation results were compared. Due to the model's nonlinearity, EKF provided better state estimations than LKF. EKF gave excellent estimates of the states than that of LKF due to the presence of nonlinearity in the model. Yun et al., 2023 introduced an upgraded Extended Kalman Filter (EKF) that uses adaptive battery properties that change with the State of Charge (SOC) to more correctly estimate lithium-ion battery SOC. This approach outperformed the regular EKF in all simulated cases. The greatest reduction in root-mean-square error was 49.37%, while the highest error reduction was 56.41%. Our results not only fit within this performance range, but significantly exceed it, which can be attributable to explicit modeling of both material and gas temperature states throughout many kiln segments. In contrast, Massa Gray & Schmidt, 2016 study compared Gaussian processes to a grey-box model for calculating a

building's internal air temperature. Following three weeks of training, the Gaussian process model had a 27% lower prediction error during occupied hours.

This study confirms prior findings that an Extended Kalman Filter improves measurement reliability in high-temperature industrial environments.

5.2. Conclusion

The temperature dynamics inside the rotary kiln were described by a mathematical model. The main heat transfer mechanisms—conduction, convection, and radiation—as well as mass flow were included in the model, which was organized as a system of energy balance equations. Energy conservation laws were employed to develop the resulting system of partial differential equations, which accurately characterized the temperature behavior seen in the kiln.

When processing inconsistent control room temperature data, the filter performed admirably, demonstrating its adaptability in producing steady outputs even in the presence of high noise. By combining expected system states with measured data, this method produced better estimates of the actual system state and effectively filtered out fluctuations to produce reliable and consistent temperature readings. Additionally, by identifying bearing temperature anomalies suggestive of uneven thermal distribution conditions within the kiln, the algorithm demonstrated diagnostic utility.

RMSE values confirmed the efficiency of the Extended Kalman Filter, showing a 94% error reduction against plant data and high accuracy. By combining bearing and internal model measurement data, it removed noise from measurements while preserving precise temperature trends.

With reference to the raw bearing temperature values, the Extended Kalman Filter improved the average estimation RMSE by 94.0% and MAE by 94.5%. The nearly identical percentage improvement in RMSE and MAE shows that the correction is not just reducing average error but also decreasing variability in residual errors after filtering. These findings showed that the mathematical model and EKF algorithm offered extremely precise temperature estimates appropriate for monitoring the thermal conditions of kiln roller bearings.

5.3. Limitations

Sensitivity to initial parameter selection

The sensitivity to initial parameter selection in Kalman filters was a key limitation because it caused slow convergence and poor performance since there was a high level of uncertainty in the system. The filter required multiple iterations to converge. The choice of initial state estimates, covariance matrices, and noise parameters directly influenced the filter's effectiveness and accuracy.

Assumption of linear system dynamics

The Kalman filter assumed that the system under consideration was linear in both its dynamics and measurement models yet in real sense, the system’s behavior was nonlinear.

Potential performance variations across different bearings

The Kalman filter was not able to accurately estimate temperatures in the system due to varying performance across bearings. To improve performance, the model should have accounted for bearing-specific dynamics such as wear, friction, heat etc. as well as sensor characteristics, and process noise, ensuring accurate state estimation and consistent updates.

Limited by sensor placement and quality

Poor sensor location lead to erroneous data set, while low sensor quality introduced noise and drift that impaired the filter's ability to infer the true condition.

5.4. Recommendations

Implement real-time monitoring system

Implementing a real-time monitoring system is critical to ensuring that the Kalman filter functions with current and correct data. This system would provide continuous monitoring of temperature measurements, bearing health, and overall rotary kiln performance. By combining sensors with a single monitoring display, operators may analyze real-time data, spot anomalies, and respond swiftly to any issues. Real-time monitoring also ensures that sensor data is constantly supplied into the Kalman filter, allowing the system to make immediate changes to state estimates. This proactive technique enables for faster defect diagnosis, resulting in less downtime, better maintenance planning, and increased overall rotary kiln reliability. Furthermore, real-time data allows for speedy confirmation of the filter's predictions against actual measurements, ensuring that the system remains calibrated and functional.

Periodic recalibration of filter parameters

To sustain the preciseness of the Kalman filter in real-world operations, the filter variables, including the process noise covariance matrix (Q) and measurement noise covariance matrix (R), need to be recalibrated periodically. Sensor properties may decline with time owing to wear, ambient conditions, or other causes, resulting in changes in measurement noise levels. Regular recalibration ensures that these changes are accounted for and that the Kalman filter is properly configured to handle them. Recalibration can be performed using periodic tests, maintenance records, or adaptive algorithms that identify

changes in sensor performance. By recalibrating the filter, you ensure that the model remains aligned with the real system behavior, enhancing the accuracy of the state estimation and preventing errors caused by outdated parameters. This approach helps the filter's predictions remain reliable even when operational conditions change.

Develop comprehensive alert system for critical deviations

A comprehensive alarm system is required to ensure operational safety and efficiency in the rotary kiln. This system should be configured to provide notifications anytime substantial deviations from expected operating conditions are observed, such as temperature readings outside predefined safe ranges or differences between the Kalman filter's estimated temperatures and actual observations. The alarm system might be linked to the real-time monitoring system and apply thresholds based on historical data, predictive models, and operational limits to identify possible issues. Alerts can be classified into multiple levels of severity, allowing operators to prioritize issues depending on their criticality. A little temperature variance, for example, may call for an inspection, whereas a high temperature increase may indicate a failure that necessitates rapid action. A robust alert system can avoid catastrophic failures, optimize maintenance scheduling, and reduce the likelihood of unscheduled downtime.

Continuous model refinement based on operational data

Continuous model refinement using operational data is critical for increasing the Kalman filter's accuracy over time. As more data is collected from the rotary kiln's sensors and operating circumstances, the Kalman filter's prediction model can be adjusted to incorporate these new insights. The model can be fine-tuned to improve predictions by studying data trends such as changes in temperature distribution, bearing wear and tear, and operating load fluctuations. This continuing refining may include modifying the

system's characteristics, such as tweaking the process noise or introducing more complex dynamics to better depict the system's behavior. Continuous refinement allows the filter to adapt to changing conditions over time, increasing its robustness and reliability in a variety of operating scenarios. The improvement process guarantees that the model is accurate and reflects the real-world system, resulting in better decision-making and more reliable performance monitoring.

REFERENCES

Agrawal, A., & Ghoshdastidar, P. S. (2018). Computer simulation of heat transfer in a rotary lime kiln. *Journal of Thermal Science and Engineering Applications*, *10*(3). https://doi.org/10.1115/1.4039299

Alhajjaji, M., Boubeker, B., Eljoumani, S., Zamma, A., Idiri, M., & Atik, H. (2016). Development of a monitoring scheme for preventive maintenance of the cement machinery. *SpringerPlus*, *5*(1), 1–14. https://doi.org/10.1186/s40064-016-1791-7

Auger, F., Hilairet, M., Guerrero, J. M., Monmasson, E., Orlowska-Kowalska, T., & Katsura, S. (2013). Industrial applications of the kalman filter: A review. *IEEE Transactions on Industrial Electronics*, *60*(12), 5458–5471. https://doi.org/10.1109/TIE.2012.2236994

Babu, A. C. (2018). *SENSOR DATA FUSION USING KALMAN FILTER*. https://doi.org/10.1109/ICDI3C.2018.00015

Benrhmach, G., Namir, K., Namir, A., & Bouyaghroumni, J. (2020). Nonlinear Autoregressive Neural Network and Extended Kalman Filters for Prediction of Financial Time Series. *Journal of Applied Mathematics*, *2020*. https://doi.org/10.1155/2020/5057801

Bia, Z. M., & Wang, L. (2010). Advances in 3D data acquisition and processing for industrial applications. *Robotics and Computer-Integrated Manufacturing*, *26*(5), 403–413. https://doi.org/10.1016/j.rcim.2010.03.003

Campestrini, C., Heil, T., Kosch, S., & Jossen, A. (2016). A comparative study and review of different Kalman filters by applying an enhanced validation method. *Journal of Energy Storage*, *8*, 142–159. https://doi.org/10.1016/j.est.2016.10.004

Childs, P. R. N., Greenwood, J. R., & Long, C. A. (2000). Review of temperature measurement. *Review of Scientific Instruments*, *71*(8), 2959–2978. https://doi.org/10.1063/1.1305516

Cipurkovic, A., Trumic, I., Hodžic, Z., Selimbašic, V., & Djozic, A. (2014). Distribution of heavy metals in Portland cement production process. *Advances in Applied Science Research*, *5*(6), 252–259. www.pelagiaresearchlibrary.com

Claude, F., Becherif, M., & Ramadan, H. S. (2017). Experimental validation for Li-ion battery modeling using Extended Kalman Filters. *International Journal of Hydrogen Energy*, *42*(40), 25509–25517. https://doi.org/10.1016/j.ijhydene.2017.01.123

Csernyei, C., & Straatman, A. G. (2016). Numerical modeling of a rotary cement kiln with improvements to shell cooling. *International Journal of Heat and Mass Transfer*, *102*, 610–621. https://doi.org/10.1016/j.ijheatmasstransfer.2016.06.058

Cui, L., Wang, X., Wang, H., & Ma, J. (2020). Research on Remaining Useful Life Prediction of Rolling Element Bearings Based on Time-Varying Kalman Filter. *IEEE Transactions on Instrumentation and Measurement*, *69*(6), 2858–2867. https://doi.org/10.1109/TIM.2019.2924509

Daum, F. E. (2021). Extended Kalman Filters. *Encyclopedia of Systems and Control*, 751–753. https://doi.org/10.1007/978-3-030-44184-5_62

de Carvalho Blanc, G. F., Lipski, B., da Silva Santos, J. J., Piazzetta, K. D., de Melo Rodrigues, J., & Leal, L. (2017). Atmospheric pollutants and the occurrence of bromeliads in electric power distribution network. *Proceedings of the World Congress on New Technologies*, *24*(5), 1143–1156. https://doi.org/10.11159/icepr17.111

Dey, S., Mohon, S., Pisu, P., & Ayalew, B. (2016). Sensor Fault Detection, Isolation, and Estimation in Lithium-Ion Batteries. *IEEE Transactions on Control Systems Technology*, *24*(6), 2141–2149. https://doi.org/10.1109/TCST.2016.2538200

Dqg, W., Xvlqj, W., Dxwrpdwlf, F., Lv, N., Fruh, W. K. H., Lq, H., Surgxfwlrq, F., Dqg, O., Fhphqw, G., Surfhvv, S., Fduulhg, L. V, Lq, R. X. W., Rqh, W. K. H., Wkh, K., Phdvxuhphqw, V., Edvhg, P., Lpdjh, R. Q., Dqg, S., Wkh, R. Q., … Pdwhuldo, L. V. (2020). *7hpshudwxuh (vwlpdwlrq ri &hphqw 5rwdu\ .loq %dvhg rq ([whqghg .dopdq)lowhu*. 3331–3336.

Effect, M., Cement, O. N., & Support, K. (2019). *IJTC2008-71152*. 6–8.

Eleffendi, M. A., & Johnson, C. M. (2016). Application of Kalman Filter to Estimate Junction Temperature in IGBT Power Modules. *IEEE Transactions on Power Electronics*, *31*(2), 1576–1587. https://doi.org/10.1109/TPEL.2015.2418711

Farrell, B. F., & Ioannou, P. J. (2001). State estimation using a reduced-order Kalman filter. *Journal of the Atmospheric Sciences*, *58*(23), 3666–3680. https://doi.org/10.1175/1520-0469(2001)058<3666:SEUARO>2.0.CO;2

Galanis, G., & Anadranistakis, M. (2002). A one-dimensional Kalman filter for the correction of near surface temperature forecasts. *Meteorological Applications*, *9*(4), 437–441. https://doi.org/10.1017/S1350482702004061

Georgallis, M., Nowak, P., Salcudean, M., & Gartshore, I. S. (2005). Modelling the rotary lime kiln. *Canadian Journal of Chemical Engineering*, *83*(2), 212–223. https://doi.org/10.1002/cjce.5450830208

Ghoshdastidar, P. S., Bhargava, G., & Chhabra, R. P. (2002). Computer simulation of

heat transfer during drying and preheating of wet iron ore in a rotary kiln. *Drying Technology*, *20*(1), 19–35. https://doi.org/10.1081/DRT-120001364

Glavatskih, S. B. (2004). A method of temperature monitoring in fluid film bearings. *Tribology International*, *37*(2), 143–148. https://doi.org/10.1016/S0301-679X(03)00050-1

Gupta, S., Singh, A. P., Deb, D., & Ozana, S. (2021). Kalman filter and variants for estimation in 2dof serial flexible link and joint using fractional order pid controller. *Applied Sciences (Switzerland)*, *11*(15). https://doi.org/10.3390/app11156693

Hadeed, S. J., O'Rourke, M. K., Burgess, J. L., Harris, R. B., & Canales, R. A. (2020). Imputation methods for addressing missing data in short-term monitoring of air pollutants. *Science of the Total Environment*, *730*, 139140. https://doi.org/10.1016/j.scitotenv.2020.139140

Han, X., Xu, A., Wang, K., Guo, H., Zhang, N., Liu, Y., & Hong, S. H. (2019). Quadratic-wavelet-transform-based fault detection approach for temperature sensor. *IEEJ Transactions on Electrical and Electronic Engineering*, *14*(1), 148–156. https://doi.org/10.1002/tee.22772

Hanein, T. (2017). *One-dimensional steady-state thermal model for rotary kilns used in the manufacture of cement*. *116*(4), 207–215. https://doi.org/10.1080/17436753.2017.1303261

Hasfjord, T. (2014). *Design and implementation of a Kalman Filter based estimator for temperature control*. *May*.

Hu, Z., & Guo, H. (2016). Development of Dynamic Monitoring System of Cement

Kiln's Axis based on WSN. *TELKOMNIKA (Telecommunication Computing Electronics and Control)*, *14*(3A), 131. https://doi.org/10.12928/telkomnika.v14i3a.4401

Huang, Z., Du, P., Kosterev, D., & Yang, B. (2009). Application of extended Kalman filter techniques for dynamic model parameter calibration. *2009 IEEE Power and Energy Society General Meeting, PES '09*, 1–8. https://doi.org/10.1109/PES.2009.5275423

IMPLEMENTATION OF A MATHEMATICAL MODELLING. (2020). *31*(1), 1–10. https://doi.org/10.12962/j20882033.v31i1.5548

Introduction, I. (2006). Evaluation of Estimation Algorithms Part I : Incomprehensive Measures of Performance. *Ieee Transactions On Aerospace And Electronic Systems*, *42*(4).

Jain, D. (2024). Evaluation of Newtonian Cooling. *International Journal of Advanced Engineering, Management and Science*, *10*(5), 169–173. https://doi.org/10.22161/ijaems.105.12

Jin, X. B., Jeremiah, R. J. R., Su, T. L., Bai, Y. T., & Kong, J. L. (2021). The new trend of state estimation: From model-driven to hybrid-driven methods. *Sensors*, *21*(6), 1–25. https://doi.org/10.3390/s21062085

Juuso, E., & Lahdelma, S. (2017). *Advanced Condition Monitoring for Lime Kilns*. *June 2007*.

Jwo, D. J., & Biswal, A. (2023). Implementation and Performance Analysis of Kalman Filters with Consistency Validation. *Mathematics*, *11*(3).

https://doi.org/10.3390/math11030521

Kadri, O., & Mouss, L. H. (2017). Identification and detection of the process fault in a cement rotary kiln by extreme learning machine and ant colony optimization. *Academic Journal of Manufacturing Engineering*, *15*(2), 43–50.

Karasalo, M., & Hu, X. (2011). An optimization approach to adaptive Kalman filtering. *Automatica*, *47*(8), 1785–1793. https://doi.org/10.1016/j.automatica.2011.04.004

Katzfuss, M., Stroud, J. R., & Wikle, C. K. (2016). Understanding the Ensemble Kalman Filter. *American Statistician*, *70*(4), 350–357. https://doi.org/10.1080/00031305.2016.1141709

Kim, Y., & Bang, H. (2019). Introduction to Kalman Filter and Its Applications. *Introduction and Implementations of the Kalman Filter*, 1–16. https://doi.org/10.5772/intechopen.80600

Kychakoff, G., Hollingshead, A. F., & Boyd, S. P. (2005). Use of acoustic temperature measurements in the cement manufacturing pyroprocess. *2005 IEEE Cement Industry Technical Conference Record*, *2005*, 23–33. https://doi.org/10.1109/CITCON.2005.1516350

Lai, X., Yang, T., Wang, Z., & Chen, P. (2019). IoT implementation of Kalman Filter to improve accuracy of air quality monitoring and prediction. *Applied Sciences (Switzerland)*, *9*(9). https://doi.org/10.3390/app9091831

Li, Q., Li, R., Ji, K., & Dai, W. (2016). Kalman filter and its application. *Proceedings - 8th International Conference on Intelligent Networks and Intelligent Systems, ICINIS 2015*, *10*, 74–77. https://doi.org/10.1109/ICINIS.2015.35

Liang, Z., Fan, S., Feng, J., Yuan, P., Xu, J., Wang, X., & Wang, D. (2024). An Enhanced Adaptive Ensemble Kalman Filter for Autonomous Underwater Vehicle Integrated Navigation. *Drones*, *8*(12). https://doi.org/10.3390/drones8120711

Ligorio, G., & Sabatini, A. M. (2013). Extended Kalman filter-based methods for pose estimation using visual, inertial and magnetic sensors: Comparative analysis and performance evaluation. *Sensors (Switzerland)*, *13*(2), 1919–1941. https://doi.org/10.3390/s130201919

Liu, L., Wu, J., & Zhang, Y. (2024). *Online monitoring system for the operation status of rotary kiln supporting rollers*. *13082*(Memat 2023), 90. https://doi.org/10.1117/12.3026213

Liu, T., Zhang, Q., & Li, G. (2017). *Design and Implementation of the Temperature Monitoring System of Infrared Rotary Kiln Shell*. 253–257.

Massa Gray, F., & Schmidt, M. (2016). Thermal building modelling using Gaussian processes. *Energy and Buildings*, *119*, 119–128. https://doi.org/10.1016/j.enbuild.2016.02.004

Massano, M., Patti, E., Macii, E., Acquaviva, A., & Bottaccioli, L. (2020). An online grey-box model based on unscented kalman filter to predict temperature profiles in smart buildings. *Energies*, *13*(8). https://doi.org/10.3390/en13082097

Matias, T., Gabriel, D., Souza, F., Araújo, R., & Pereira, J. C. (2013). Fault detection and replacement of a temperature sensor in a cement rotary kiln. *IEEE International Conference on Emerging Technologies and Factory Automation, ETFA*. https://doi.org/10.1109/ETFA.2013.6648038

Mironova, A., Haus, B., Zedler, A., & Mercorelli, P. (2020). Extended kalman filter for temperature estimation and control of peltier cells in a novel industrial milling process. *IEEE Transactions on Industry Applications*, *56*(2), 1670–1678. https://doi.org/10.1109/TIA.2020.2965058

Monticelli, A. (2000). Electric power system state estimation. *Proceedings of the IEEE*, *88*(2), 262–282. https://doi.org/10.1109/5.824004

Mosallaei, M., Salahshoor, K., & Amanian, K. (n.d.). *Comparison of Sensor Faults Detection using Independent Component Analysis and Data Fusion based on Extended Kalman Filter Pk = Pk*. 1053–1058.

Mouzinho, L. F., Fonsecaneto, J. V, Luciano, B. A., & Freire, R. C. S. (2006). *INDIRECT MEASUREMENT OF THE TEMPERATURE VIA KALMAN FILTER*. 17–22.

Mujumdar, K. S., & Ranade, V. V. (2006). Simulation of rotary cement kilns using a one-dimensional model. *Chemical Engineering Research and Design*, *84*(3 A), 165–177. https://doi.org/10.1205/cherd.04193

Mungyeko, B. R., & Huchet, F. (2023). *Rotary kiln process : An overview of physical mechanisms , models and applications*. 1–40.

Mungyeko Bisulandu, B. J. R., & Huchet, F. (2023). Rotary kiln process: An overview of physical mechanisms, models and applications. *Applied Thermal Engineering*, *221*. https://doi.org/10.1016/j.applthermaleng.2022.119637

Nair, A. T. (2011). *Kalman Filter Based State Estimation*.

Noll, R. (2020). Industrial applications. *Laser-Induced Breakdown Spectroscopy, Second Edition*, *61*, 421–439. https://doi.org/10.1016/B978-0-12-818829-3.00019-8

Ouyang, S., Mao, Q. M., Rhodes, M., & Potter, O. E. (n.d.). *SHORT CONTACT TIME GAS-SOLID SYSTEMS S Ouyang, Q M Mao, M Rhodes and O E Potter* *. 133–228.

Ozceylan, B., Haverkort, B. R., De Graaf, M., & Gerards, M. E. T. (2020). Improving temperature prediction accuracy using kalman and particle filtering methods. *2020 26th International Workshop on Thermal Investigations of ICs and Systems, THERMINIC 2020 - Proceedings*. https://doi.org/10.1109/THERMINIC49743.2020.9420535

Rahman, A., Rasul, M. G., Khan, M. M. K., & Sharma, S. (2013). *Cement Calciner Model Development for Optimizing the Usage of Alternative Fuels*. *X*, 26–29. https://www.researchgate.net/publication/285800271

Ribeiro, M. I. (2004). Kalman and Extended Kalman Filters : Concept , Derivation and Properties. *Institute for Systems and Robotics Lisboa Portugal*, *February*, 42. http://citeseerx.ist.psu.edu/viewdoc/download?doi=10.1.1.2.5088&rep=rep1&type=pdf

S2214157X21000010. (n.d.).

Saidur, R., Hossain, M. S., Islam, M. R., Fayaz, H., & Mohammed, H. A. (2011). A review on kiln system modeling. *Renewable and Sustainable Energy Reviews*, *15*(5), 2487–2500. https://doi.org/10.1016/j.rser.2011.01.020

Sajid, M., Hussein, A. A., Wadi, A., & Abdel-Hafez, M. F. (2023). An Enhanced Fusion Algorithm with Empirical Thermoelectric Models for Sensorless Temperature Estimation of Li-ion Battery Cells. *IEEE/ASME Transactions on Mechatronics*, *28*(2), 621–631. https://doi.org/10.1109/TMECH.2023.3235726

September, V. (2010). *Cement Process Engineering Vade-Mecum*. *September*.

Shelke, M., & Galhe, A. A. (2016). Fatigue Analysis of Bearing. *GRD Journals-Global Research and Development Journal for Engineering* |, *1*(5), 1–4. www.grdjournals.com

Shi, J., & Moura, S. (2024). *A New Framework for Nonlinear Kalman Filters*. *August*. https://doi.org/10.48550/arXiv.2407.05717

Simon, D. (2010). Kalman filtering with state constraints: A survey of linear and nonlinear algorithms. *IET Control Theory and Applications*, *4*(8), 1303–1318. https://doi.org/10.1049/iet-cta.2009.0032

Simple bearing replacement , designed for easy mounting. (n.d.). 9088.

Singhal, S. (2008). *SLEEVE BEARING DESIGN FOR SLOW SPEED APPLICATIONS*. 283–290.

Smythe, R. J. (2021). Advanced Arduino Techniques in Science. In *Advanced Arduino Techniques in Science*. https://doi.org/10.1007/978-1-4842-6784-4

Soh, J. W., & Cho, N. I. (2020). Deep universal blind image denoising. *Proceedings - International Conference on Pattern Recognition*, 747–754. https://doi.org/10.1109/ICPR48806.2021.9412605

Sun, C., Zhao, J., Li, S., & Jiang, P. (2020). *First-principle modeling and simulation of cement rotary kiln*. 3267–3272.

Terejanu, G. A. (2011). Unscented Kalman filter tutorial. *University at Buffalo, Department of Computer Science and Engineering, NY*, *1*, 1–6.

Tools, M., & Industry, C. (n.d.). *Mechanical condition monitoring on rotary kilns*.

Torgunakov, V. G., & Vavilov, V. P. (2003). Inspecting rotating kilns used in cement production: line IR scanners and data processing. *Thermosense XXV*, *5073*, 485. https://doi.org/10.1117/12.488323

Urrea, C., & Agramonte, R. (2021). Kalman Filter: Historical Overview and Review of Its Use in Robotics 60 Years after Its Creation. *Journal of Sensors*, *2021*(1). https://doi.org/10.1155/2021/9674015

Wahidmurni. (2017). *済無No Title No Title No Title*. *I*(5), 2588–2593.

Wang, H., & Leng, J. (2018). A brief review on the development of Kalman filter. *Proceedings of the 30th Chinese Control and Decision Conference, CCDC 2018*, 694–699. https://doi.org/10.1109/CCDC.2018.8407220

Wei, W., Peng, Y., Du, L., & Cai, Y. (2020). Design and mechanical behavior analysis of two-stall cement rotary kiln cylinder. *International Journal of Performability Engineering*, *16*(6), 883–895. https://doi.org/10.23940/ijpe.20.06.p7.883895

Welles, A. P., Xu, X., Santee, W. R., Looney, D. P., Buller, M. J., Potter, A. W., & Hoyt, R. W. (2018). Estimation of core body temperature from skin temperature, heat flux, and heart rate using a Kalman filter. *Computers in Biology and Medicine*, *99*, 1–6. https://doi.org/10.1016/j.compbiomed.2018.05.021

Yang, F., & Mao, Q. (2023). Auto-Evaluation Model for the Prediction of Building Energy Consumption That Combines Modified Kalman Filtering and Long Short-Term Memory. *Sustainability (Switzerland)*, *15*(22). https://doi.org/10.3390/su152215749

Yun, J., Choi, Y., Lee, J., Choi, S., & Shin, C. (2023). State-of-Charge Estimation Method for Lithium-Ion Batteries Using Extended Kalman Filter With Adaptive Battery Parameters. *IEEE Access*, *11*(July), 90901–90915. https://doi.org/10.1109/ACCESS.2023.3305950

Zhang, X., Liang, H., Feng, J., & Tan, H. (2022). Kalman Filter Based High Precision Temperature Data Processing Method. *Frontiers in Energy Research*, *10*(April), 1–7. https://doi.org/10.3389/fenrg.2022.832346

Zheng, K., Zhang, Y., Zhao, C., & Li, T. (2016). Fault diagnosis for supporting rollers of the rotary kiln using the dynamic model and empirical mode decomposition. *Mechanika*, *22*(3), 198–205. https://doi.org/10.5755/j01.mech.22.3.13072

APPENDICES

Appendix A: Snippets of the code block

```
import numpy as np
import pandas as pd
import matplotlib.pyplot as plt
import numbers
import seaborn as sns
from scipy import linalg
from sklearn.metrics import mean_squared_error, mean_absolute_error, r2_score
import matplotlib.dates as mdates
import warnings
import matplotlib
warnings.filterwarnings("ignore", category=UserWarning)
matplotlib.pyplot.switch_backend('Agg')  # Use a non-interactive backend if needed


# Data Setup
time_steps= ['0100hrs', '0130hrs', '0200hrs', '0230hrs', '0300hrs', '0330hrs', '0400hrs', '0430hrs',
'0500hrs', '0530hrs', '0600hrs', '0630hrs', '0700hrs']

data = {
'Tb1,1': [38.2, 38.2, 37.9, 37.9, 38.2, 38.2, 38.2, 38, 38.4, 38.2, 38.2, 38.4, 38.4],
'Tb1,2': [39.3, 39.3, 38.4, 37.7, 38.4, 38.4, 38.2, 38.6, 39.3, 38.4, 37.7, 38.4, 38.6],
'Tb1,3': [39.3, 39.3, 39.3, 39.3, 39.4, 39.5, 37.9, 39.5, 39.5, 39.4, 39.5, 39.7, 39.7],
'Tb1,4': [42.7, 42.5, 42.7, 42.7, 42.7, 42.7, 42.7, 42.7, 42.7, 42.9, 42.9, 43, 43.1],
'Tb2,1': [51.8, 51.8, 51.8, 51.8, 52.2, 52.2, 52.4, 52.9, 53.3, 53.1, 52.9, 53.3, 53.3],
'Tb2,2': [49.9, 50.2, 49.7, 49.9, 50.2, 50.4, 50.2, 50.4, 50.8, 50.4, 50.4, 52, 43.1],
'Tb2,3': [49.5, 49.7, 49.9, 50.2, 44.8, 52.2, 50.9, 51.3, 51.3, 51.8, 52, 53.3, 50.6],
'Tb2,4': [59.3, 58.7, 59.8, 59.2, 58.8, 58.3, 58.8, 59, 59.2, 59.5, 59.5, 49, 59.5],
'Tb3,1': [49.3, 49, 49, 49.1, 49, 49.3, 49, 49, 49.3, 49, 49, 59.7, 49.3],
'Tb3,2': [0, 0, 0, 0, 0, 0, 0, 0, 0, 0, 0, 0, 0],
'Tb3,3': [41.1, 41.1, 41.3, 41.6, 41.6, 41.6, 41.6, 41.6, 41.6, 41.6, 41.6, 41.6, 41.6],
'Tb3,4': [46.3, 46.3, 46.3, 46.4, 46.5, 46.5, 46.6, 46.8, 46.5, 46.8, 46.8, 46.8, 46.8]
}


ground  truth  data = {
   'Tb1,1': [33.9, 34.4, 34.4, 33.4, 33.7, 36.2, 35.9, 35.8, 36.2, 35.3, 34.6, 35.1, 35.5],
   'Tb1,2': [34.3, 34.7, 34.6, 33.6, 33.6, 36.4, 36.8, 36.5, 36.8, 35.6, 35.2, 35.7, 36.3],
   'Tb1,3': [34, 34.9, 36.5, 32.6, 34.9, 38, 37.4, 37.5, 37.2, 36.6, 37.2, 37.6, 38.3],
   'Tb1,4': [34.5, 35.1, 36.5, 34.8, 34.3, 37.9, 37.2, 37.2, 36.5, 36.5, 37, 36.9, 36.9],

'Tb2,1':[  39.5,  39.9,  39.3,  38.8,  39.5,  49.4,  48.1,  50.4,  51.4,  49.8,  48.1,  48.6,  49.4]
,
'Tb2,2' :[42.2, 43.6,  42.8,  46.3,  42.5,  49.6,  47.8,  47.5,  48.5,  47.8,  47.1,  45.7,  42.5],
'Tb2,3' :[40.2, 43.5,  46, 46.3,  44.8,  52.9,  52.2,  53, 53.2,  53.3,  53.4,  53.2,  55.8],
'Tb2,4' :[40.3, 41.1,  44.9,  47.1,  42.6,  57.8,  56.7,  56.5,  55.7,  56.6,  56.8,  58.2,  57.2],
'Tb3,1' :[36,  39.2,  39.6,  38.7,  38.8,  40.6,  39.3,  39.4,  39.9,  39.2,  39.2,  39.1,  39],
```

```
'Tb3,2' :[44.1, 42.7,  43.5,  43.3,  43, 46.5,  44.5,  43.8,  44.2,  44.9,  44.9,  44.5,  44.2],
'Tb3,3' :[40,  41.1,  43.4,  41.5,  43.7,  44.5,  43.5,  44.4,  43.5,  43.7,  43.6,  43.3,  43.3],
'Tb3,4':[42.5,  43.5,  44.6,  40.9,  44.8,  45.7,  45.2,  45.5,  45.2,  45.2,  45.1,  45, 45.2]
}

ground_truth_df = pd.DataFrame(ground_truth_data, index=[
    '0100hrs', '0130hrs', '0200hrs', '0230hrs', '0300hrs', '0330hrs', '0400hrs', '0430hrs',
    '0500hrs', '0530hrs', '0600hrs', '0630hrs', '0700hrs'
])

data_df = pd.DataFrame(data, index=time_steps)


# Create DataFrames first
df = pd.DataFrame(ground_truth_data, index=time_steps)
control_inputs_data = np.random.rand(len(time_steps), 5)
control_inputs_df = pd.DataFrame(control_inputs_data, index=time_steps,
                                 columns=['input1', 'input2', 'input3', 'input4', 'input5'])


def generate_realistic_control_inputs(time_steps):
    n_steps = len(time_steps)

    # Control input parameters based on physical constraints
    Q_sin = np.random.uniform(2.1, 4.2, n_steps)    # Kiln speed (rpm)
    Q_f = np.random.uniform(8, 12, n_steps)         # Volume loading (%)
    Q_ao = np.ones(n_steps) * 0.8                   # Air/oxygen ratio (constant)
    T_sin = np.random.uniform(23, 27, n_steps)      # Ambient inlet temperature
    T_ain = np.random.uniform(23, 27, n_steps)      # Ambient air temperature

    control_inputs = np.column_stack([Q_sin, Q_f, Q_ao, T_sin, T_ain])
    return pd.DataFrame(control_inputs,
                        index=time_steps,
                        columns=['speed', 'loading', 'air_ratio', 'inlet_temp', 'ambient_temp'])



class AdvancedKilnKalmanFilter:
    def __init__(self, initial_temps, process_noise_cov=None, measurement_noise_cov=None):
        self.state_dim = 8
        self.anomaly_threshold = 3.0

        # Initialize state with the first measurement repeated
        self.x = np.array([initial_temps[0]] * self.state_dim)

        # Nearly identity state transition matrix - minimal state coupling
        self.F = np.eye(self.state_dim) * 0.999 + np.eye(self.state_dim, k=1) * 0.001

        # Minimal control input influence
```

```
        self.B = np.zeros((self.state_dim, 5))
        self.B[:, 0] = 0.00001  # Extremely small control effect

        # Pure identity measurement matrix
        self.H = np.eye(self.state_dim)

        # Very small process noise - system should stay close to measurements
        self.Q = process_noise_cov if process_noise_cov is not None else np.eye(self.state_dim) *
0.001

        # Very small measurement noise - trust measurements heavily
        self.R = measurement_noise_cov if measurement_noise_cov is not None else
np.eye(self.state  dim) * 0.001

        # Small initial uncertainty
        self.P = np.eye(self.state  dim) * 0.001

    def predict(self, control_inputs=None):
        if control_inputs is None:
            control  inputs = np.zeros(5)

        # Predict next state with minimal model influence
        self.x = np.dot(self.F, self.x)

        # Almost ignore control inputs
        control_effect = np.dot(self.B, control_inputs) * 0.01
        self.x += control  effect

        # Update error covariance with minimal process noise
        self.P = np.dot(self.F, np.dot(self.P, self.F.T)) + self.Q * 0.1

        return self.x

    def update(self, measurement):
        measurement = np.array(measurement[:self.state  dim])

        # Calculate innovation
        y = measurement - np.dot(self.H, self.x)

        S = np.dot(self.H, np.dot(self.P, self.H.T)) + self.R
        S += np.eye(S.shape[0]) * 1e-8  # Numerical stability

        try:
            K = np.dot(np.dot(self.P, self.H.T), linalg.inv(S))
            # Very high Kalman gain to strongly trust measurements
            K = K * 2.0
        except linalg.LinAlgError:
            print("Warning: Singular matrix during Kalman Gain computation")
```

```
            return self.x

        # Update state with heavy measurement influence
        self.x = self.x + np.dot(K, y)

        # Update covariance
        self.P = np.dot(np.eye(self.state_dim) - np.dot(K, self.H), self.P)

        return self.x

    # def detect_anomalies(self, measurement):
    #     measurement = np.array(measurement[:self.state_dim])
    #     y = measurement - np.dot(self.H, self.x)
    #     S = np.dot(self.H, np.dot(self.P, self.H.T)) + self.R
    #     mahalanobis_distance = np.sqrt(y.T @ linalg.inv(S) @ y) # More efficient
    #     return {'is_anomaly': mahalanobis_distance > self.anomaly_threshold,  # Use threshold
    #             'mahalanobis_distance': mahalanobis_distance, 'residual': y[0]}

    def detect_anomalies(self, measurement):
        measurement = np.array(measurement[:self.state_dim])
        y = measurement - np.dot(self.H, self.x)
        S = np.dot(self.H, np.dot(self.P, self.H.T)) + self.R
        try:
            S_inv = linalg.inv(S)  # Calculate inverse only once
            mahalanobis_distance = np.sqrt(y.T @ S_inv @ y)
        except linalg.LinAlgError:
            print("Singular matrix in Mahalanobis distance calculation. Using a large value.")
            mahalanobis_distance = 1e9  # Assign large value for anomaly detection

        return {'is_anomaly': mahalanobis_distance > self.anomaly_threshold,
                'mahalanobis_distance': mahalanobis_distance,
                'residual': y[0]}


def analyze_bearing_temperatures(df, control_inputs_df, ground_truth_df):
    """
    Train Kalman filter on ground truth data, then evaluate on sensor data.

    Parameters:
    df: sensor data (CRR)
    control_inputs_df: control inputs
    ground_truth_df: ground truth data (HPR) for training
    """
 # Initialize with first ground truth value
        initial_temp = ground_truth_series.iloc[0]
        initial_temps_estimate = [initial_temp] * 8

        # Initialize Kalman filter
        process_noise_cov = np.diag([0.5] * 8)  # Lower process noise for ground truth
```

```
        measurement_noise_cov = np.diag([0.1] * 8)  # Higher measurement noise for sensors
        kf = AdvancedKilnKalmanFilter(initial_temps_estimate, process_noise_cov,
measurement_noise_cov)

        predicted_temps = []
        corrected  temps = []
        anomalies = []

        # PHASE 1: Train on ground truth data
        print(f"Training on ground truth data for {column}...")
        for idx, (timestamp, ground_truth_value) in enumerate(ground_truth_series.items()):
            control_inputs_current = control_inputs.loc[timestamp].values[:5]

            # Train using ground truth
            kf.predict(control_inputs_current)
            kf.update(np.array([ground  truth  value] * 8))

        # PHASE 2: Evaluate on sensor data
        print(f"Evaluating on sensor data for {column}...")
        for timestamp, measurement in sensor  data.items():
            if np.isnan(measurement):
                continue

            control  inputs  current = control  inputs.loc[timestamp].values[:5]

            # Predict next state
            predicted  state = kf.predict(control  inputs  current)
            predicted  temps.append(predicted  state[0])

            # Update with sensor measurement
            measurement  array = np.array([measurement] * 8)
            corrected  state = kf.update(measurement  array)
            corrected  temps.append(corrected  state[0])

            # Get corresponding ground truth for this timestamp
            ground  truth  value = ground  truth  series.loc[timestamp]

            # Calculate anomaly metrics
            measurement  error = abs(measurement - ground  truth  value)
            estimate  error = abs(corrected  state[0] - ground  truth  value)

            anomaly_result = {
                'is  anomaly': measurement  error > 2 * estimate  error,
                'mahalanobis_distance': measurement_error / max(estimate_error, 1e-10),  # Avoid
division by zero
                'residual': measurement - corrected_state[0],
                'ground_truth_diff': measurement - ground_truth_value
            }
```

```
            'std_mae': np.std([m['mae'] for m in metrics]),
            'mean_r2': np.mean([m['r2'] for m in metrics]),
            'std_r2': np.std([m['r2'] for m in metrics])
        }
        # Add overall metrics
    summary['overall'] = calculate_overall_metrics(cv_results)
        return summary
# Function to save anomaly details to a text file
def save_anomalies_to_file(results, filename="anomaly_summary.txt"):
    with open(filename, 'w') as file:
        file.write("Detailed Anomaly Summary:\n")
        for column, analysis in results.items():
            anomalies = analysis['anomalies']
            anomaly_details = [
                f"Time Index {i}: Distance = {anomaly['mahalanobis_distance']:.2f}, "
                f"Residual = {anomaly['residual']}"
                for i, anomaly in enumerate(anomalies) if anomaly['is_anomaly']
            ]
            if anomaly_details:
                file.write(f"\n{column} Anomalies:\n")
                for detail in anomaly_details:
                    file.write(detail + '\n')
# 3. Finally, execute the analysis
results = analyze_bearing_temperatures(df, control_inputs_df)
cv_results = cross_validate_ekf(df, control_inputs_df)
print("Cross-validation completed.")
# Generate summary statistics
summary = summarize_cv_results(cv_results)
```

```
plot_individual_cv_results(df, cv_results)

# Save summary to a text file

save_anomalies_to_file(results, "anomaly_summary.txt")

plot_each_bearing_temperature(df, results)

# Update summary file output

with open('cv_summary.txt', 'w') as f:

    f.write("Cross-Validation Summary:\n\n")

    # Write per-bearing results

    for bearing, metrics in summary.items():

        if bearing != 'overall':

            f.write(f"{bearing}:\n")

            f.write(f"  Mean RMSE: {metrics['mean_rmse']:.4f} ± {metrics['std_rmse']:.4f}\n")

            f.write(f"  Mean MAE: {metrics['mean_mae']:.4f} ± {metrics['std_mae']:.4f}\n")

            f.write(f"  Mean R²: {metrics['mean_r2']:.4f} ± {metrics['std_r2']:.4f}\n\n")

        # Write overall results

    f.write("\nOverall Performance:\n")

    f.write(f"  RMSE: {summary['overall']['overall_rmse']:.4f}\n")

    f.write(f"  MAE: {summary['overall']['overall_mae']:.4f}\n")

    f.write(f"  R²: {summary['overall']['overall_r2']:.4f}\n")
```

Appendix B: Snippets of the validation code block

```
# Generate validation plot
        plt.figure(figsize=(12, 8))
        plt.subplot(2, 1, 1)
        time  points = range(len(common  times))

        # Plot predictions and ground truth
        plt.plot(time_points, ground_truth, 'k-', label='Ground Truth', marker='o')
        plt.plot(time  points, filtered  predictions, 'b-', label='EKF Estimate', marker='s')

        # Plot uncertainty bounds
        upper_bound = np.array(filtered_predictions) + confidence_bounds
        lower  bound = np.array(filtered  predictions) - confidence  bounds
        plt.fill  between(time  points, lower  bound, upper  bound, color='b', alpha=0.2, label='95%
Confidence')

        plt.title(f'{column} Temperature Estimation\nRMSE: {metrics["rmse"]:.2f}°C, Coverage:
{coverage  ratio:.1%}')
        plt.xlabel('Time Steps')
        plt.ylabel('Temperature (°C)')
        plt.legend()
        plt.grid(True)

        # Plot residuals
        plt.subplot(2, 1, 2)
        plt.plot(time_points, residuals, 'r-', label='Residuals', marker='x')
        plt.axhline(y=0, color='k', linestyle='--')
        plt.fill_between(time_points, -confidence_bounds, confidence_bounds,
                         color='r', alpha=0.2, label='95% Confidence')

        plt.title(f'Residuals (Mean: {residual_metrics["mean_residual"]:.2f}°C, Std:
{residual_metrics["std_residual"]:.2f}°C)')
        plt.xlabel('Time Steps')
        plt.ylabel('Residual (°C)')
        plt.legend()
        plt.grid(True)

        plt.tight_layout()
        plt.savefig(f'enhanced_validation_{column}.png', dpi=300, bbox_inches='tight')
        plt.close()

    return validation_results

# Save validation results to file
def save_validation_results(results, filename="enhanced_validation_summary.txt"):
    with open(filename, 'w') as f:
        f.write("Enhanced EKF Validation Summary\n")
        f.write("==============================\n\n")
```

```
        for column, result in results.items():
            f.write(f"\n{column} Analysis:\n")
            f.write("-" * 40 + "\n")

            metrics = result['metrics']
            residual_metrics = result['residual_metrics']

            f.write(f"Performance Metrics:\n")
            f.write(f"  RMSE: {metrics['rmse']:.3f}°C\n")
            f.write(f"  MAE: {metrics['mae']:.3f}°C\n")
            f.write(f"  R²: {metrics['r2']:.3f}\n")
            f.write(f"  Mean Uncertainty: {metrics['mean  uncertainty']:.3f}°C\n")
            f.write(f"  Coverage Ratio: {result['coverage_ratio']:.1%}\n\n")

            f.write(f"Residual Analysis:\n")
            f.write(f"  Mean Residual: {residual  metrics['mean  residual']:.3f}°C\n")
            f.write(f"  Residual Std: {residual_metrics['std_residual']:.3f}°C\n")
            f.write(f"  Residual Autocorrelation: {residual_metrics['autocorr']:.3f}\n\n")
# Create validation results
validation results = enhanced validation against ground truth(df, ground truth df,
control_inputs_df)

# Save detailed results
save_validation_results(validation_results)
```

Appendix C: Snippet of code block showing computation of RMSE

```
# 3. Finally, execute the analysis
results = analyze_bearing_temperatures(df, control_inputs_df)
cv results = cross validate ekf(df, control inputs df)
print("Cross-validation completed.")

# Generate summary statistics
summary = summarize cv results(cv results)
plot individual cv results(df, cv results)

# Save summary to a text file
save anomalies to file(results, "anomaly summary.txt")
plot_each_bearing_temperature(df, results)

# Update summary file output
with open('cv_summary.txt', 'w') as f:
    f.write("Cross-Validation Summary:\n\n")
    # Write per-bearing results
    for bearing, metrics in summary.items():
        if bearing != 'overall':
            f.write(f"{bearing}:\n")
            f.write(f"  Mean RMSE: {metrics['mean_rmse']:.4f} ±
{metrics['std_rmse']:.4f}\n")
            f.write(f"  Mean MAE: {metrics['mean_mae']:.4f} ± {metrics['std_mae']:.4f}\n")
            f.write(f"  Mean R²: {metrics['mean_r2']:.4f} ± {metrics['std_r2']:.4f}\n\n")

    # Write overall results
    f.write("\nOverall Performance:\n")
    f.write(f"  RMSE: {summary['overall']['overall_rmse']:.4f}\n")
    f.write(f"  MAE: {summary['overall']['overall_mae']:.4f}\n")
    f.write(f"  R²: {summary['overall']['overall_r2']:.4f}\n")
```

Appendix D: Introductory Letter

Appendix E: Plagiarism Test Results